PHYSICAL MONITORING OF THE SOUTH FORK MCKENZIE RIVER: EXPLORING THE USE OF UNOCCUPIED AIRCRAFT SYSTEMS TO ASSIST FIELD-BASED MONITORING.

Final Project Report
submitted to the
McKenzie Watershed Alliance

17 August 2022

in partial fulfillment of reporting requirements
for Grant #220-7000-17342 from the
Oregon Watershed Enhancement Board
and titled
"Evaluating Ecological and Geomorphic Responses to Stage 0 Restoration"

prepared by

Steve Wondzell[1], Jon Burnett[2], Matt Barker[3], Sarah Hinshaw[4], Michael Wing[5], and Wyatt McCurdy[6]

1. Research Ecologist, US Forest Service, Pacific Northwest Research Station, Corvallis Forestry Sciences Laboratory, Corvallis OR 97331.
2. Research Forester, US Forest Service, Pacific Northwest Research Station, Olympia Forestry Sciences Laboratory, Olympia WA 98512.
3. Doctoral Student, Forest Engineering, Resources & Management Department, Aerial Information Systems Lab, College of Forestry, Oregon State University, Corvallis OR 97331.
4. Doctoral Student, Geosciences Department, Warner College of Natural Resources, Colorado State University, Ft. Collins, CO 80523.
5. Associate Professor, Forest Engineering, Resources & Management Department, Aerial Information Systems Lab, College of Forestry, Oregon State University, Corvallis OR 97331.
6. Remote Sensing Analyst, RedCastle Resources Inc/under contract to the USDA Forest Service Geospatial Technology Applications Center.

EXECUTIVE SUMMARY

We explored the use of unoccupied aircraft systems (UAS) to monitor the South Fork McKenzie River (SFMR) after it had undergone restoration to a Stage-0 condition. One of the primary goals of restoration to a Stage-0 condition is to create complex valley floor environments that can be subsequently reshaped by natural processes, and in this case, to allow those natural processes to build high-quality habitat for salmon in what was an anthropogenically altered river reach below a large flood-control reservoir. Restoration to the Stage-0 condition follows the Stream Evolution Model of Cluer and Thorne (2014). More than 60 ha of the channel and floodplain of the SFMR was treated by re-grading the channel and floodplain to a "geomorphic grade line" as described by Powers et al., (2019). The actual restoration of the 900-m long reach involved using 65,000 m^3 of sediment scraped from levied channel banks and other high portions of the floodplain to raise the channel bed and reconnect flows onto the floodplain. Thousands of large logs were added during restoration, and the ends of some logs were buried in the sediment to provide foundations for future log jams.

Effectiveness monitoring is an important aspect of any restoration, and especially so here, given the relative novelty of the Stage-0 methods. However, monitoring using traditional channel-based protocols was made difficult by the large-scale of the SFMR project, the lack of a distinct channel, and the expectation of substantial future geomorphic processes that will reshape the floodplain and future development of riparian vegetation. We considered these challenges as opportunities to test new monitoring protocols based on newly available technologies based on UASs. We used a DJI Matrice 300 equipped with a MicaSense Altum multispectral camera and a DJI Phantom 4 Pro UAS to investigate approaches for quantitative remote sensing. Specifically, we quantified inundated area, amounts of large instream wood, sediment size, water surface velocity, and water temperature from UAS photogrammetry, thermography, and multispectral orthomosaics. The UAS surveys were coordinated with paired field measurements for all metrics except inundated area to calibrate and validate the remotely sensed data.

Here, we describe our monitoring protocols, present our preliminary results, and discuss issues with the remote sensing and evaluate its capacity to monitor post-treatment changes at the restored site. Overall, distributions of velocity, temperature, and large wood overlapped with paired field data, signifying a possible relationship, however, there was insufficient paired data to conduct hypothesis testing. UAS data collection costs were $1/10^{th}$ the cost of field data collection costs and UAS data density were many orders of magnitude higher, yet when accounting for technical and practical barriers to implementation and analysis, a clear advantage becomes elusive. In terms of efficacy, four of the five factors were generally successful, but all methods require more refinement before operational implementation is reasonable. UAS remote sensing methods provide more data and more spatial coverage, but additional data and more process refinement is necessary before operational implementation is recommended.

Table of Contents

GENERAL INTRODUCTION

Degraded floodplains and valley floors are restored with the goal of enhancing habitat for native fish and aquatic-riparian biota and the protection or improvement of water quality. Recent years have seen a shift toward "process-based restoration" that is intended to reestablish compromised eco-geomorphic processes resulting from site- or watershed-scale degradation. One form of process-based restoration developed in the Pacific Northwestern United States has been increasingly implemented in recent years. This restoration approach is intended to reconnect rivers to their floodplains by slowing down flows of sediment, water, and nutrients to encourage their lateral and vertical connectivity at base flows, facilitating development of dynamic, self-forming, and self-sustaining river-wetland corridors. Synergies between applied practices and theoretical work have led this form of restoration to be referred to regionally as restoration to a Stage-0 condition (Cluer and Thorne, 2014).

The restoration of significant lengths of the riverbed and valley floor of the South Fork McKenzie River (SFMR) to a Sage-0 condition used the Geomorphic Grade Line approach (Powers et al., 2019). The channel and floodplain were graded to match the average slope of the valley. Some 65,000 m^3 of sediment were redistributed from leveed banks and other high portions of the floodplain, intentionally filling the existing channel. Floodplain roughness was increased to slow water velocity by adding nearly 4000 large logs, many with rootwads, some of which were partially buried to limit potential for high flows to transport large wood off the site. These restoration activities dramatically increased the inundated area and complexity of the newly formed aquatic habitat. However, the large spatial extent and abundant large wood presents significant challenges for post-restoration monitoring. Access is difficult and wading is dangerous and potentially life threatening at high flows. Existing monitoring protocols are primarily designed for single-thread channels, and while they can be adapted to include secondary or back channels, they are difficult if not impossible to apply where extensive portions of the floodplain are inundated, and no distinct "channel" may be present. Further, conventional field methods such as plots or transects may not adequately characterize the spatial heterogeneity on a site as complex as SFMR.

The ready availability of unoccupied aircraft systems (UAS), relatively inexpensive, high-resolution multi-spectral sensors, and the ubiquity of software for image processing offers an alternative to traditional, field-based methods for monitoring. The primary objective of this project was to explore the use of UAS in monitoring post-restoration changes at two "Stage-0" restoration sites: Whychus Creek located near Sisters OR and the South Fork McKenzie River located near Rainbow OR. Of course, more traditional field validation data were necessary to test UAS-based methods. Consequently, our project used a combination of field validation plots and repeated UAS flights to monitor the two study sites for several years post-restoration. We employed identical UAS-based surveys and similar field validation methods. Here, we focus on both the UAS monitoring at the South Fork McKenzie River restoration site and results from field plots and measurements designed to validate the UAS monitoring.

The UAS monitoring focused on 5 specific factors, all of which were expected to change, both in response to the initial restoration treatment, and in the subsequent years and decades as

the channel and valley floor responded to the suite of biological and geomorphological processes jump-started through restoration to a Stage-0 condition. These 5 factors are: (1) inundated area, (2) flow velocity, (3) large wood, (4) sediment, and (5) stream temperature.

This report only covers a short period of time following the active restoration. We expect that the channels and valley floor will change over time, as the immediate post-restoration constructed surfaces are modified by natural geomorphic and biological processes. As such, the data collected in these first years of monitoring provide a foundation for future studies from which the long-term trajectory of change can be evaluated.

Overview of Methods

Stage-0 restoration design was implemented along the lower portion of the South Fork McKenzie River (SFMR), Oregon. The McKenzie River Sub-basin is located within the larger Willamette River Basin. River water is composed of rain and snowmelt and cold spring-fed water making this river system one of the last locations in the Willamette Basin capable of supporting cold water dependent species such as bull trout (*Salvelinus confluentus*) and spring Chinook salmon (*Oncorhynchus tshawytsha*).

The restoration project is located directly downstream of an existing flood control dam and impounded reservoir (Cougar Dam and Reservoir). Levees, berms, and other structures that were built to channelize the stream and provide floodplain staging areas during the construction of Cougar Dam significantly altered the ability of the mainstem channel to interact with the floodplain. Prior to restoration, the channel planform was predominantly a single thread channel with some simplified secondary channel areas.

The restoration of the SFMR began during the summer of 2018. The restoration was planned in three initial phases, starting at the tributary junction of the South Fork with the mainstem McKenzie and moving upstream. Phase I was implemented in 2018, Phase II in 2019, and Phase III was planned for the summer of 2021 (Table 1). The SFMR Stage-0 monitoring project was subdivided into several topical areas, each with a somewhat independent sampling design. For example, eDNA and macro-invertebrate sampling begin in the Phase I area in 2017 and continued through 2019 and allowed for a pre- vs post-restoration analysis. In contrast, the food-web study, with independent sampling of macro-invertebrates and fish diet compositions did not start until 2019. This work in the Phase I area contrasted data from the unrestored Phase III to compare restored vs unrestored reaches. The Phase IV area was also sampled, so than after the Phase III area was restored, a full before-after, control-impact (BACI) design would be available for analyses. Unfortunately, the SAR-COV2 pandemic and the Holiday Farm Fire of September 2020 has altered restoration plans and delayed implementation of Phase III and subsequent phases.

The physical / biogeomorphic UAS based monitoring captured a few pre- and during-restoration surveys, but the associated intensive field monitoring did not begin until the summer of 2019, one-year after the completion of the Phase I restoration. Thus, lack pre-restoration data for most metrics that we monitored. Further, we concentrated our efforts in the Phase I

restoration reach and did not monitor un-restored reaches located immediately above the Phase I reach.

Aerial Survey with Unoccupied Aircraft Systems

The UAS aerial surveys were flown twice each year, targeting a spring flight at high flows before leaf-out and a late summer flight under low flow conditions. UAS airframes and sensor combinations were determined by UAS availability, and perceived risk determined by environmental conditions and the flight profile for each task (Table 2). Flights were contracted to the Aerial Information Systems Laboratory at Oregon State University. For the 2018 – 2021 period of this work, the USFS PNWRS did not have organic capacity or authority to conduct UAS surveys.

Two different airframes were used to support this study. A DJI Matrice 200 which has a 24- to 34-minute endurance and can lift about 1.5 kg (Figure 1). The second UAS used was a DJI Phantom 4 Pro (Figure 2) with an attached data logger, Inertial Measurement Unit, GPS receiver, and laser rangefinder to produce accurate altimeter measurements of aircraft height above ground as in Dawson et al. (2017). This is necessary because the aircraft's altimeter produces a barometric altitude in units of height above mean sea level, that is internally converted to a localized height AGL at the aircraft's initialization point (typically the takeoff location or home point) which is likely inaccurate because elevation at the study site is not uniform across the entire area of interest.

South Fork McKenzie River Biological Studies

PHASE I	2017			2018			2019					2020				2021			
	PRE-RESTORATION			RESTORATION			POST-RESTORATION					POST-RESTORATION				POST-RESTORATION			
		eDNA	Kick Inverts		eDNA	Kick Inverts		eDNA	Kick Inverts	FWeb Inverts	Fish Diet		eDNA	FWeb Inverts	Fish Diet		eDNA	FWeb Inverts	Fish Diet
	Winter			Winter			Winter					Winter		Y	Y	Winter		Y	Y
	Spring			Spring	Jun-19	Jun-19	Spring	June-19	Jun-19			Spring		Y	Y	Spring		Y	Y
	Summer			Summer			Summer			Y	Y	Summer		Y	Y	Summer			
	Fall	Oct-17	Oct-17	Fall			Fall	Oct-19	Oct-19	Y	Y	Fall		Y	Y	Fall			

Restoration work active - no sampling
Before-After Restoration Comparison
Space-for-Time Restoration Comparison
Trophic Basis for Production (Food Web)

PHASE II: Summer

PHASE III	2017			2018			2019					2020				2021				WY2022				WY2023			
	PRE-RESTORATION			PRE-RESTORATION			PRE-RESTORATION					PRE-RESTORATION				RESTORATION				POST-RESTORATION				POST-RESTORATION			
		eDNA	Kick Inverts		eDNA	Kick Inverts		eDNA	Kick Inverts	FWeb Inverts	Fish Diet		eDNA	FWeb Inverts	Fish Diet		eDNA	FWeb Inverts	Fish Diet		eDNA	FWeb Inverts	Fish Diet		eDNA	FWeb Inverts	Fish Diet
	Winter			Winter			Winter					Winter		Y	Y	Winter		Y	Y	Winter		Y	Y	Winter		Y	Y
	Spring			Spring	Jun-19	Jun-19	Spring	June-19	Jun-19			Spring		Y	Y	Spring		Y	Y	Spring		Y	Y	Spring		Y	Y
	Summer			Summer			Summer			Y	Y	Summer		Y	Y	Summer				Summer		Y	Y	Summer		Y	Y
	Fall	Oct-17	Oct-17	Fall			Fall	Oct-19	Oct-19	Y	Y	Fall		Y	Y	Fall		Y	Y	Fall		Y	Y	Fall		Y	Y

PHASE IV	2019				2020				2021				2022				2023			
	PRE-RESTORATION				PRE-RESTORATION				PRE-RESTORATION				PRE-RESTORATION				RESTORATION			
		eDNA	FWeb Inverts	Fish Diet		eDNA	FWeb Inverts	Fish Diet		eDNA	FWeb Inverts	Fish Diet		eDNA	FWeb Inverts	Fish Diet		eDNA	FWeb Inverts	Fish Diet
	Winter				Winter		Y	Y	Winter		Y	Y	Winter		Y	Y	Winter		Y	Y
	Spring				Spring		Y	Y	Spring		Y	Y	Spring		Y	Y	Spring		Y	Y
	Summer		Y	Y	Summer		Y	Y	Summer		Y	Y	Summer		Y	Y	Summer			
	Fall		Y	Y	Fall		Y	Y	Fall		Y	Y	Fall		Y	Y	Fall		Y	Y

Table 1: Summary of restoration and monitoring activities as developed for the initial study plan at the beginning of the project in 2019.

Type	UAS	Camera	Date	Phase	Target Flow	Ortho-mosaic Processed	DSM Processed	Sediment Processed	Inundation Processed	Velocity Processed	Wood Processed	Thermal Processed	Discharge (m^3/s)
Aerial Survey	DJI Phantom 4	RGB	5/1/18	1	High	Y	Y						9.7
Aerial Survey	DJI Phantom 4	RGB	7/1/18	1	Low	Y	Y						9.0
Aerial Survey	DJI Phantom 4	RGB	8/17/18	1	Low	Y	Y		Y				9.3
Aerial Survey	Matrice 200 v2	Altum	10/1/18	1*	Low	Y	Y						9.9
Aerial Survey	DJI Phantom 4	RGB	10/1/18	3	Low	Y	Y						9.9
Aerial Survey	DJI Phantom 4	RGB	4/19/19	1	High	Y	Y		Y				137.6
Photo/Video Plots	DJI Phantom 4	RGB	8/27/19 [F]	1	Low			Y		Y			23.9
Aerial Survey	Matrice 200 v2	Altum	8/26/19 [F]	1	Low	Y	Y						23.9
Aerial Survey	Matrice 200 v2	Altum	9/23/19	1	Low	Y	Y		Y		Y		14.7
Photo/Video Plots	DJI Phantom 4	RGB	9/23/19	1	Low			Y		Y			14.7
Aerial Survey	Matrice 200 v2	Altum	4/21/20	1	High	Y	Y		Y				11.8
Aerial Survey	Matrice 200 v2	Altum	4/23/20	2	High	Y	Y						11.5
Photo/Video Plots	DJI Phantom 4	RGB	9/4/20 [F]	1	Low			Y		Y		Y	14.2
Aerial Survey	Matrice 200 v2	Altum	9/3/20 [F]	2	Low	Y	Y						14.2
Aerial Survey	Matrice 200 v2	Altum	9/4/20 [F]	1	Low	Y	Y		Y				14.2
Aerial Survey	Matrice 200 v2	Altum	10/29/20	2	Low	Y	Y						23.8
Aerial Survey	Matrice 200 v2	Altum	11/4/20	1	Low	Y	Y		Y				23.1
Photo/Video Plots	DJI Phantom 4	RGB	7/14/21 [F]	1	Low			Y		Y			10.9
Aerial Survey	Matrice 200 v2	Altum	7/15/21 [F]	1	Low	Y	Y						10.9
Aerial Survey	Matrice 200 v2	Altum	7/16/21 [F]	2	Low	Y	Y						11.0
Aerial Survey	Matrice 200 v2	Altum	5/22/22	1*	High	Y	Y						34.3

Definitions

*	Partial area collection
[F]	Indicates Field data collected within five days of survey
Type - Aerial Survey	Flight at 400' (120 m) above ground level to survey large area in order to create orthomosaic
Type - Photo/Video Plots	Pre-selected locations to capture low altitude image and video for detailed analysis
Camera - RGB	Stock RGB True color red, green, blue sensitive camera that is stock to the UAS
Camera - Altum	Micasense Altum 6 band multispectral sensor that includes two NIR bands and 1 LWIR (thermal) band
Target Flow	Relative discharge in terms of high or low; where winter/spring typically corresponds with high flows
Phase	Pre-defined restoration planning areas on SFMR
Processed	Data are prepared for follow-on analysis
Discharge (m^3/s)	Discharge as measured at Rainbow gaging station at 12:00 Pacific Daylight Time day on date in Date column

Table 2 (Preceding page): Summary of UAS surveys conducted at the SFMR between May 2018 and May 2022.

Figure 1: Matrice 200 with Altum Multispectral Sensor – yellow circle identifies incident light sensor

Figure 2 - Phantom 4 Pro. Laster altimeter not shown.

Two different sensors were employed depending on the flight profile and UAS available. The MicaSense Altum sensor, which is a 6-band multispectral imager with narrowband red (R), green (G), blue (B), red edge (RE), near infrared (NIR), and longwave infrared (LWIR; i.e. thermal) sensors. At 120 m AGL this sensor produces images with ground sampling distances (GSDs) of 5.4 cm in the R, G, B, RE, and NIR bands, and 81 cm in the LWIR band. Because of the sensor's size and external power requirements it was exclusively mounted and flown onboard the DJI Matrice 200 (Figure 1). At the time of purchase the sensor was approximately $10,000. The Altum employs an incident light sensor (as seen in Figure 1) and a spectral calibration panel (not shown) that was always employed during each flight in accordance with the manufacturer's recommended procedure. The Altum was specifically selected for this project due to the presence of a LWIR image that facilitates the simultaneous collection of color and thermal imagery (Figure 3). The second sensor was the stock camera on the DJI Phantom 4 which is a CMOS camera with a color Bayer filter array that produces three broadband R, G, B true color images, that when combined into a single image, approximately replicates color as perceived by the human eye, and produces images at 3.3 cm GSD at 120 m AGL.

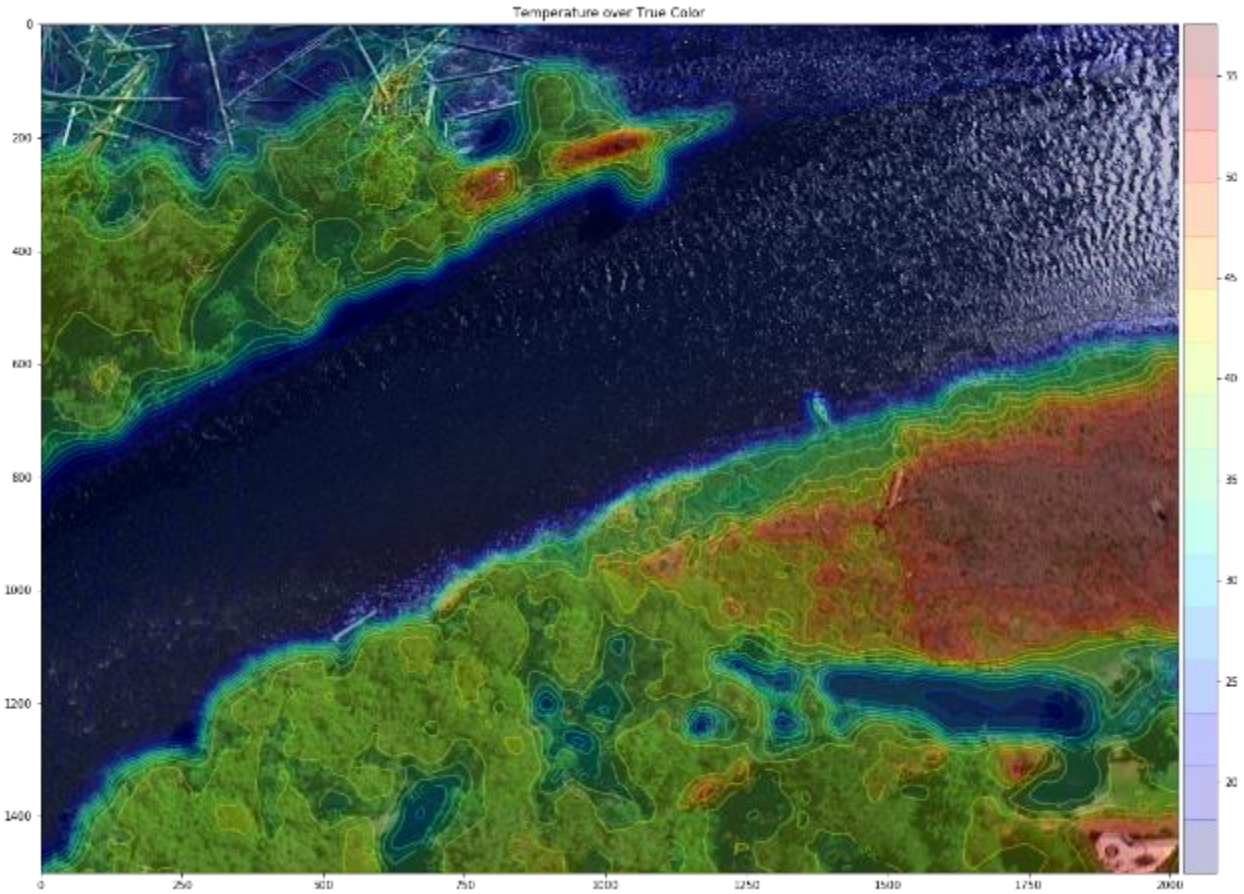

Figure 3: Thermal contours overlaid on color Imagery at south fork McKenzie River. Color legend for temperature in degrees C is on the right side.

Two distinctly different flight profiles were flown: an aerial survey profile (Figure 5a) and a photo/video plot profile (Figure 5b). The aerial survey profile was a continuous, full areal extent survey flown to produce orthomosaics of the entire area of interest. Areas of interest were coarsely defined as Phase 1, Phase 2, and Phase 3. Prior to flying, eight spatially dispersed ground control points were established with a survey grade GNSS using iron cross aerial survey targets (Figure 4) that were visible from the air. The flight profile was such that the UAS climbed to an altitude of approximately 120 m AGL, flew a lawnmower pattern and captured numerous overlapping images of the area of interest with the attached camera to produce stereo imagery (Figure 5a), then landed at the starting point. Stereo imagery facilitated the subsequent processing of images through Agisoft Metashape structure-from-motion (SFM) software to produce both an orthomosaics and a digital surface model. Both the Phantom 4 and Matrice 200 + Altum were flown in the aerial survey profile as specified in Table 2. The Altum was not available in summer 2018 so the Phantom 4 was flown. Additionally, spring high flow surveys were considered high risk to the Altum sensor due to the possibility of rainfall, so the Phantom 4 was exclusively used on those surveys as well. All aerial surveys were planned and executed using DJI GS Pro software on a tablet.

Photo/video plots profiles were point-based surveys where the UAS climbed to an altitude of 120 m, navigated to a given point (Figure 5b), descended to the specified altitude, collected imagery, returned to 120 m AGL, and repeated these steps until all points were surveyed or battery reached 15% capacity. Photo/video plots were intended to support collection of three specific metrics (flow velocity, large wood, and sediment grain size) that we planned to extract in subsequent analyses. Once at the point, the UAS collected a 10-second 4k resolution video and 20-megapixel image while hovering 7 m above the ground, resulting in image resolution of 0.2 cm GSD. These very high-resolution images were designed to enable measurement of large woody material, bed texture, and sediment size distribution. A second 10 second video and image (0.6 cm GSD) was acquired from 20 m above the ground and was intended to measure flow velocity and direction. Note that 100 of these photo/video plots were planned, with 40 being co-located with field validation plots (described later), however, due to time constraints, line of sight limitations, and radio signal degradation when dropping below canopy, only the 40 co-located with field survey plots were flown (Table 2). Note that the field survey plots were typically sampled 24 – 48 hours prior to the photo/video plot flight and heavily flagged, but the flagging was rarely visible to the pilot due to glint and grainy video transmission, so in many cases the photo/video plot only partially aligned with the field survey plot. These flights did not occur during the spring high flow survey because of poor lighting due to oblique sun angles at the mid-latitude of the study site, and due to high flows and white-water obscuring many of the logs and sediment patches of interest. These flights necessitated the aircraft to dip below the forest canopy. Given the potential concern of lost link or collision with trees, the lower cost DJI Phantom IV was used exclusively for these surveys. Note that a longer focal length camera would have been preferable to dipping below the canopy to ensure the requisite image resolution was met. However, with higher altitude comes increased likelihood for atmospheric distortions, tree branches, and subtle aircraft movements that cause blurring. Planning of these flights utilized DJI GS Pro software, and the resulting display was used by the pilot to guide aircraft flight operations. However, due to the inherently challenging nature of imaging below the tree canopy, flights were conducted using the fly-by-wire capability of the aircraft. The details of the field validation plot establishment and measurement are reported below (see the sub-section

titled: "*Short-term changes on field validation plots*"). Further, these details are relevant to the subsections on flow velocity, large wood, and streambed sediment size distributions.

Figure 4: Iron Cross aerial survey target

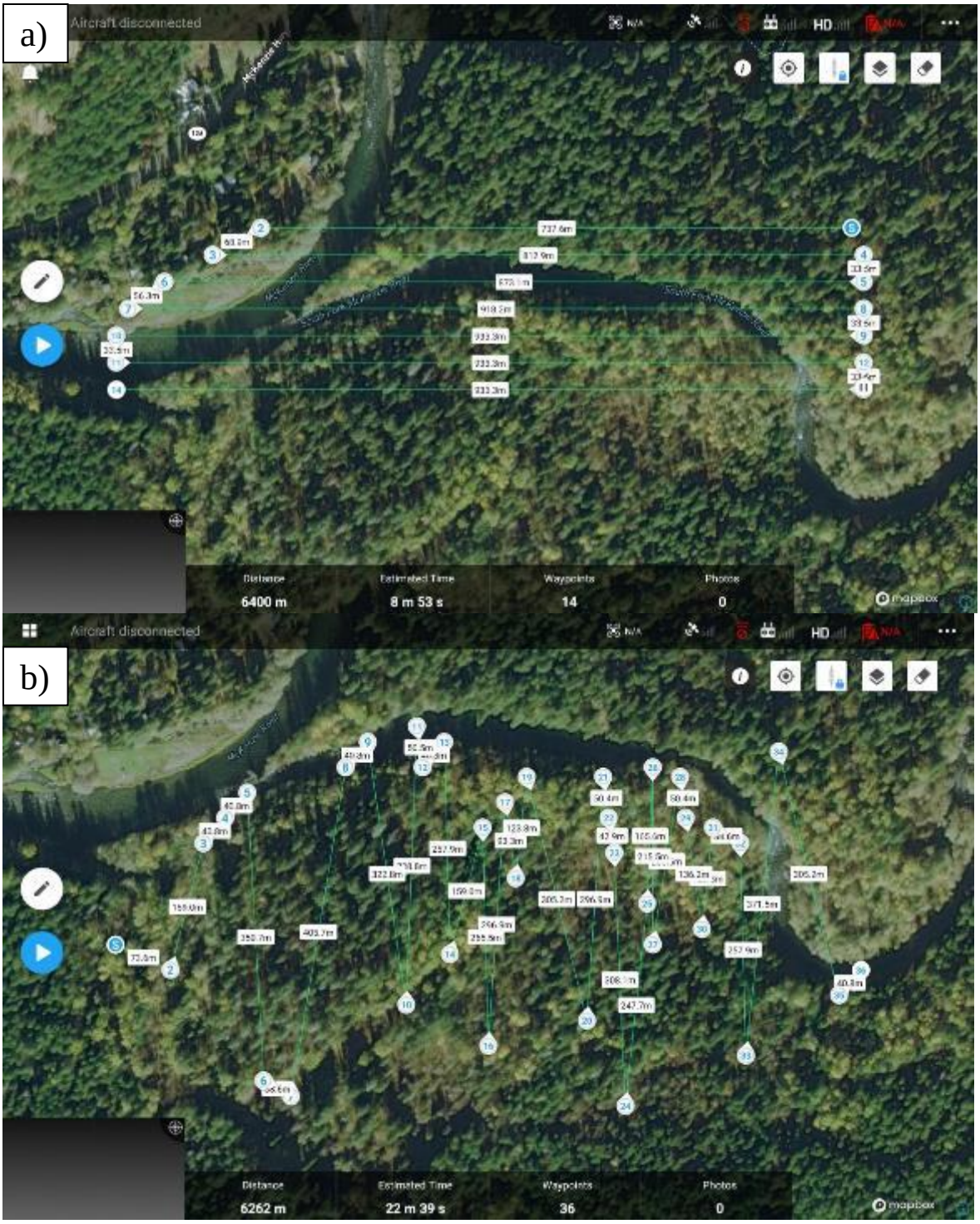

Figure 5: Flight profiles. a) Aerial survey profile over Phase I as viewed in the DJI GS Pro application. b) Overview of the Photo/video plot profile in the DJI GS Pro application.

SUB-PROJECT-REPORTS

Short-term changes on field validation plots[1]

(Reporting work led by Sarah Hinshaw and Ellen Wohl, Colorado State University)

Introduction – Field Validation Plots:

We designed the field geomorphic monitoring strategy to be easily accessible, statistically viable, and to pair well with remote sensing data. We chose to measure geomorphic field plots, rather than traditional transects, because plots are more likely to capture diverse scales of spatial heterogeneity that are an emphasis of restoration at the site. In addition, the increasing availability of monitoring with drones allows most plan-view, and sometimes vertical, hydraulic geometry variables to be estimated remotely with aerial imagery.

We do not have pre-restoration plot data from the site because our plots were established after the site was treated. Consequently, we cannot directly compare pre- and post-restoration site characteristics and we focus our analyses on changes occurring in the first 2 years following restoration. We evaluate changes in each of the variables listed earlier. Initial conditions immediately after restoration largely reflect the placement of large wood and anthropogenic disruption of topography and sediment distribution. With time, geomorphic processes will presumably redistribute sediment, as well as large wood and particulate organic matter, creating associated changes in substrate, hydraulics (flow depth and velocity), wood volume, and organic cover.

Methods – Field Validation Plots:

Our geomorphic sampling design includes 40 hexagonal plots randomly located within the Phase I restoration reach. Individual plots were selected randomly from a 4000-plot tessellation overlaid on the 0.6 km^2 area (Figure 6). Each plot has an area of 51.46 m^2 and contains four 1-m-radius circular subplots (Figure 7). Plots are distinguished as either interfluve forested land (not flooded at typical high flows) or surface inundated at high flow (which includes the active channel). We chose 40 plots to pilot the monitoring strategy as a means of balancing time constraints and the need for a sufficiently large dataset for statistical analyses. Field measurements were collected from the plots at approximately the same time as the UAS survey to provide a validation dataset against which the UAS-based estimates could be compared.

[1] Please note that most of the text in this subsection of the report is copied (sometimes with slight modification) from: *Hinshaw, S., E. Wohl, J. D. Burnett, and S. Wondzell. 2022. Development of a geomorphic monitoring strategy for Stage-0 restoration in the South Fork McKenzie River, Oregon, USA. Earth Surface Processes and Landforms* (available at https://doi.org/10.1002/esp.535615).

Figure 6: Plot locations in the Phase 1 restoration reach of the South Fork McKenzie River.

The design of the geomorphic monitoring plots was based on US Forest Service Forest Inventory and Analysis protocols (Bechtold & Patterson, 2005). We used a two-stage cluster sampling design in which geomorphic field plots are the primary sampling units and subplots within geomorphic field plots are secondary sampling units. Thus, each 51.46 m^2 hexagon was divided into four subplots: one center subplot, and three outer subplots, the centers of which are located 3 m from the center at azimuths 30°, 150°, and 270° (Figure 7). In the field, the survey team navigated to the center plot location using a 0.3 m horizontal accuracy EOS Arrow 100 GNSS receiver and used a tape and compass to determine the outer subplot locations. The design of four closely spaced subplots allows for analysis of spatial heterogeneity at multiple levels of proximity.

At each subplot we measured large wood volume, percent organic cover, water depth and velocity, canopy cover, and substrate. Velocity was measured at both the surface and 60% depth to identify differences between surface and deeper water. Water depth, velocity, and canopy cover were measured at the center of the subplot and were expected to represent the average of the 3.14 m^2 area. Organic cover, large wood, and substrate measurements covered the entire subplot, and were measured via trained visual estimation, diameter and length measurements, and a random 10-clast sample, respectively. We chose these variables because they represent easily measured components of aquatic ecosystems (Baron et al., 2002).

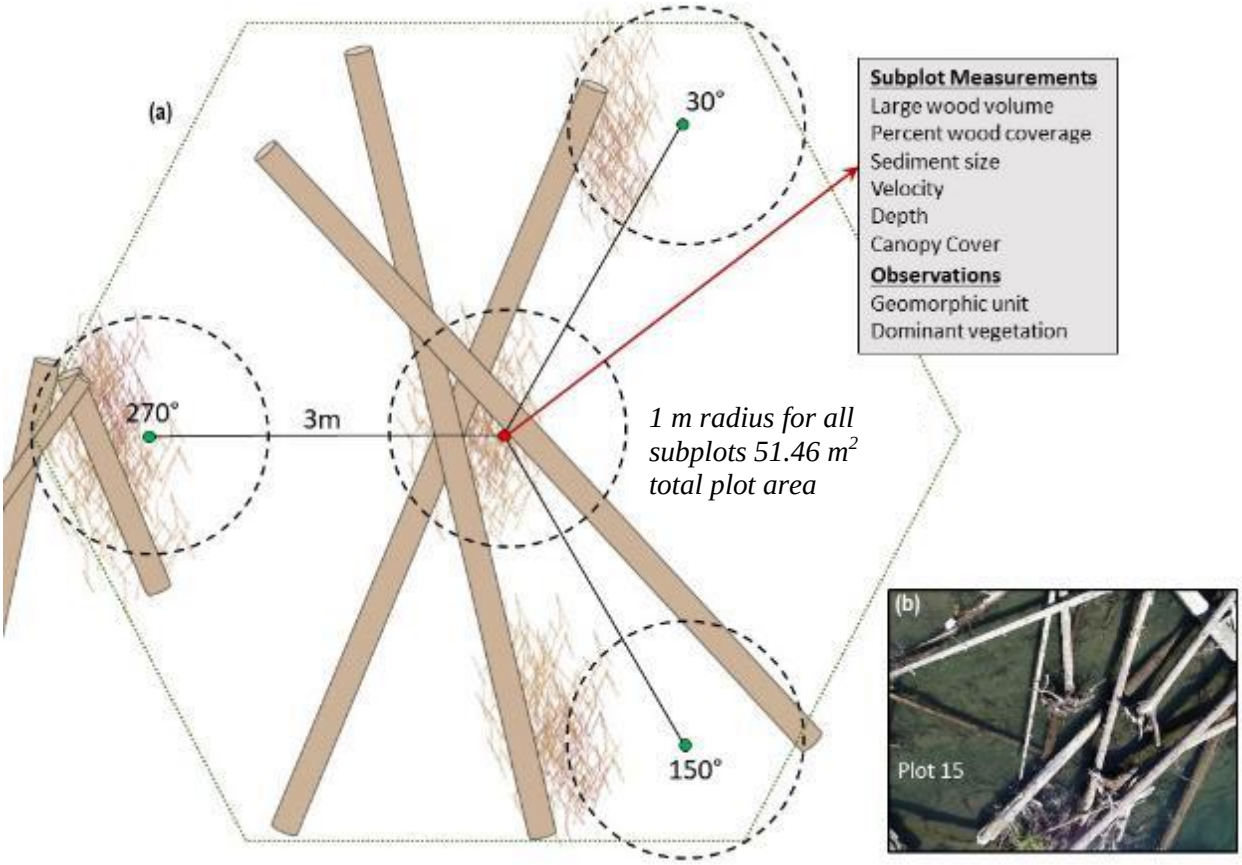

Figure 7: (a) Layout of geomorphic field plot. Outer subplots are distributed around the center subplot at 30°, 150°, and 270° azimuths. (b) A photograph example of a geomorphic field plot with overlay of plot design.

An identical set of measurements was collected at each of the four subplots. However, we slightly modified the field sampling protocol in 2020, adding the large wood measurements in all three of the outer subplots. Previously, these data were only collected in the central subplot (Figure 7). At each 1-m radius subplot, we measured canopy cover with a modified 17-point spherical densiometer in each cardinal direction; water depth with an engineer's rule; velocity at the surface and 60% flow depth using a Marsh–McBirney one-dimensional (1D) velocimeter; the size of each piece of large wood that intersected the plot, using a metric tape for piece diameter and TruPulse 360° laser range finder for piece length; and sediment size via gravelometer with 10 randomly selected clasts per subplot. Because field surveys took place in July–August 2019 and August 31–September 4, 2020, we expect there to be no change in canopy due to seasonal differences. Finally, we used categorical sediment data in a non-parametric difference test, and power analysis to evaluate the number of geomorphic field plots needed to optimize the field monitoring strategy presented here.

Floodplain spatial heterogeneity is well established as an important component of biologically and geomorphically functioning river corridors. However, methods of measuring

floodplain heterogeneity are inconsistent in the literature. We used the intra-class correlation coefficient, also called the intra-cluster correlation coefficient (ICC), to assess the correlation among subplots within a plot compared to the correlation between plots throughout the entire site. We also used the ICC to assess heterogeneity at the intermediate inter-plot scale.

Results – Field Validation Plots:

Changes in the first years following restoration: Canopy cover decreased significantly from 2019 to 2020 according to the clustered Welch two-sample t-tests (Table 3). Aside from the non-parametric test for sediment described later in this section, no other measured variables experienced statistically significant changes over the two measurement years. Results for significant differences in sediment using the nonparametric test were obtained from tests of the total sediment dataset and from the compiled medians of each set of 10 clasts per subplot ($p < 0.001$ for the entire dataset and the dataset of subplot medians). The non-parametric test does detect sufficient evidence to conclude that there is a significant difference in grain size between 2019 and 2020 (Table 3).

Table 3: Estimates for the mean values of measured variables 2019–2020 and associated standard error.

Variable	2019	2020	P-value
Canopy cover (%)	40±6	26±6	$p < 0.0001$
Organic cover (%)	20±3	23±4	$p = 0.33$
Wood volume center subplot (m^3)	2.8±0.4	2.4±0.3	$p = 0.40$
Median grain size (mm)	37±8	33±8	$p = 0.37$
Wilcoxon Signed Rank Test			$p < 0.0001$
Water velocity at surface (m/s)	0.16±0.04	0.16±0.04	$p = 0.98$
Water velocity at 60% depth (m/s)	0.15±0.04	0.14±0.03	$p = 0.67$
Water depth (cm)	26.4±4.6	23.0±3.8	$p = 0.19$

Spatial Heterogeneity: The ICC increased for all variables in the intra-plot analyses between 2019 and 2020, except for organic cover, indicating that canopy cover, substrate, water velocity, and water depth became more spatially homogeneous at the intra-plot scale. In contrast, the ICC for organic cover, sediment size, and water depth decreased from 2019 to 2020, suggesting that the spatial heterogeneity of these variables increased at distances up to 100 m between the paired plots. The ICC of the paired plots was smaller than the intra-plot ICC, indicating that among-plot heterogeneity was greater than within-plot heterogeneity in both years for all variables except sediment size in 2019 and organic cover in 2020. For these, heterogeneity is higher when examined at the intra-plot scale.

Evaluation of the field-monitoring strategy: We detected fining in categorical sediment classes between 2019 and 2020 ($p = 0.01$). Using the same test over multiple iterations, we found that the non-parametric power analysis with categorical sediment data reaches 80% power at 60 plots. Based on sediment data alone, 60 plots each year are required to ensure > 80% statistical

power to detect a change in sediment size. With the current study design of 40 plots, we achieve 67% power to detect differences in substrate classes.

Discussion – Field Validation Plots:

Changes in the first years following restoration: Between 2019 and 2020 we observed a 35% loss of tree canopy cover. Surveys were completed in July–August 2019 and August 31–September 4, 2020, so canopy cover decrease due to seasonal change alone is unlikely. We did observe many dead trees as well as many newly toppled trees in 2020, which likely explained the loss of canopy cover. There are multiple potential causes. Channel filling raised water levels across the entire floodplain of the SFMR, including persistent rises in the water table and flooding in many areas, killing many large trees. Also, large areas of the site were opened during the restoration, leaving remaining trees more exposed to the wind. Finally, flooding and high water tables might have softened the soils so that trees were less wind-firm after restoration.

Coarse particulate organic matter (CPOM) can be a critical foundation to the foodweb, supporting primary consumers. The SFMR is a large, poorly shaded river, and the restoration greatly expanded the wetted area and perhaps changed the relative importance of allochthonous versus autochthonous CPOM. However, we see strong changes in organic cover with flow distance through the restoration site. Our data suggest that CPOM is efficiently trapped in the upper portion of the study area but lost in the lower portion of the study area. Between construction in 2018, and consecutive years of measurement in 2019 and 2020, organic material deposited before restoration on dry forest floor was inundated, reworked, and transported, especially in the reactivated secondary channel in the southern portion of the restoration site. Longitudinal connectivity of CPOM has thus decreased within the upstream portion of the study area and increased in the downstream portion. The explanation for this difference in CPOM retention between the upstream and downstream portions of the study area is not known but could involve the steeper gradient of the downstream portion or the more efficient transport of CPOM within the reactivated secondary channel in the downstream portion.

We do not see a pattern of fining substrate similar to that of accumulating organic cover at upstream plots. Organic material transported from upstream, especially material mobilized by upstream restoration, was likely trapped at the surface by placed large wood pieces and constructed log jams, while fine sediment carried in suspension downstream is distributed throughout the site. Although the proportion of gravels did not significantly increase, the proportion of gravel in both years is higher than the proportion of cobbles and boulders, providing more spawning opportunity than the primarily boulder-bedded condition prior to restoration. We assume that the increase in sand is temporary and associated with disturbance from restoration activities upstream, based on the increased sand proportion, our field observations of Phase I during upstream construction, and direct observation of construction activity in Phase II. In a connectivity context, longitudinal connectivity of fine sediment has decreased, allowing local deposition of fine sediment and creating spawning habitat.

Spatial Heterogeneity: ICCs with intra-plot and intermediate-scale inter-plot data reveal changes in spatial heterogeneity and provide evidence that, at a scale of tens of meters, habitat is stabilizing in a pattern that reflects local-scale controls. The channel restoration and regrading of the valley floor by heavy equipment destroyed the previous armor layer and fill materials mixed

deeper sediment layers and floodplain surface sediment so that the as-built restored surface was much finer textured. The restoration was completed in late summer of 2018 and our first post-restoration measurements were collected in 2019, after winter high flows had already started reworking the sediment. Local processes have continued to rework this sediment and our plot data reflect the changes that occurred between 2019 and 2020.

Heterogeneity decreased at the intra-plot scale for all the metrics we measured except organic cover. At the intermediate-scale, heterogeneity increased for organic cover, substrate, and water depth. Organic cover and substrate also had increased variance when calculated for the entire site. These increases in diversity reflect promising trends in local-scale habitat availability for organisms throughout multiple life cycle stages.

Qualitative observations suggest that restoration activities at the study site have altered connectivity. The direct addition of substantial large wood and the resulting formation of an anastomosing channel planform have reduced longitudinal connectivity within the channel. Removal of artificial levees and regrading of channel and floodplain surfaces have increased lateral connectivity. The combined effects of more in-channel obstructions from large wood and the greater inundated surface area have likely increased vertical connectivity. These changes to 3D connectivity better represent natural conditions in river corridors of this region prior to intensive human alteration starting in the 19th century.

Evaluation of the field-monitoring strategy: The monitoring protocols we developed for the SFMR were intended to serve as a pilot that could be modified to better capture geomorphic change and complexity and to allow monitoring of other ecological and remotely sensed metrics. We recognize that the monitoring approach presented here has room for improvement, but think it is important to share with the broader scientific community in effort to begin the process of establishing best practices for Stage-0 restoration monitoring through replication, repetition, expansion to new sites and regions, and inspiration of new methods.

This protocol in particular is designed to complement a suite of remote sensing methods where similar measurements can be obtained from UASs and subsequently calibrated using field measurements. Once calibrated, future iterations of remote monitoring can be implemented in a low-cost, time-efficient manner with seasonal or annual frequency adapted to local needs. In the meantime, field-based monitoring methods that aim to eliminate bias and capture spatial heterogeneity are useful in the initial evaluation of large-scale projects such as the one described at SFMR.

Based on our power analysis and the results from the ICC analysis, we suggest that simple random sampling might provide a better alternative than the two-stage cluster sampling design we employed here. Having a single plot (or a single subplot within a plot) is reasonable because of the relative homogeneity we observed within clusters when compared to heterogeneity throughout the site. This modification would also increase statistical power for determining changes through time, because, for the same effort, field crews could substantially increase the number of plots sampled. For example, a sample size of $n = 60$ plots with only one subplot per plot would provide a balance of statistical viability and field feasibility. However, the tradeoff

for replacing clustered plots with single subplots is a limited ability to capture small-scale heterogeneity.

Inundated Area

Introduction – Inundated Area:

One of the critical goals of restoring a valley floor and stream corridor to a Stage-0 condition is to enhance the connectivity between the stream and its flooplain. Connectivity, however, involves the interaction of materials (sediment, water, organic matter), energy (flow velocity, stream power, and sunlight), or organisms. Further, connectivity can be assessed across different scales, and in three critical dimensions – longitudinal, lateral, and vertical. Here we consider the longitudinal and lateral connectivity of water across the entire channel and floodplain surface.

In many streams and rivers throughout the inter-mountain west, and elsewhere throughout the world, the long history of anthropomorphic changes has increasingly isolated streams from their floodplains. This severance of natural connectivity has impacted many ecosystem processes and the consequent services that these ecosystems provide society. Restoration to a Stage-0 condition reverses these trends. At the SFMR, the massive restructuring of the valley floor and channel have both raised the elevation of the channel bed and lowered the elevation of the highest surfaces of the floodplain. No distinct channel remains and large portions of the valley floor are inundated, even at low flow discharges. The changes in the overall wetted area and patterns of floodplain inundation have implications for the amount of aquatic habitat, as well as vegetation response, thermal conditions and groundwater. Here, we explored the use of UAS imagery to map the extent of the wetted, or inundated, area within the Phase I restoration area.

Methods – Inundated Area:

Multi-spectral ortho-imagery of the South Fork McKenzie River restoration site was used to map the inundated area and wetted edge. Pre-restoration data was derived from the 2016 Oregon State Imagery Program data collected in early summer 2016, and post restoration data was collected in late summer 2020, with a small UAS. The whole of the analysis was completed using ArcGIS Pro (ver. 2.4, ESRI Corp., Redlands, CA). Inundated area was estimated using the supervised classification tool and a Normalized-Difference Vegetation Index (NDVI) derived from the imagery for each year.

Follow-up processing was required for the post-treatment estimate. The extent of the inundated area was often complex, with narrow channels that were partially obscured by overhanging vegetation, emergent macrophytes, and floating or suspended logs. In these cases, the water surface was occluded in the UAS imagery. Occluded inundation area was estimated by using elevation model (DEM) derived from Light Detection and Ranging (LiDAR) data collected in early-summer 2020 to create a Height Above Nearest Drainage (HAND; Nobre et al. 2011) surface. A maximum vertical change of 0.3 m was heuristically determined to best capture inundated area in the occluded areas based on congruence to inundated area estimate from imagery and analyst's recollection of conditions in occluded channels. The result was combined with the non-overlapping components of the inundated area estimate data to create a more complete post-treatment estimate of inundated area. Pre- and post- restoration wetted edge was estimated by calculating the perimeter of the respective inundated area using ArcGIS. Finally, wetted edge complexity was quantified with a ratio index where the denominator is the perimeter

of a hypothetical circle having a given inundated area and the numerator is the wetted edge associated with the given inundated area.

Results – Inundated Area:

The post-restoration inundated area was estimated to be 153,719 m^2, nearly four times larger than the inundated area of 41,144 m^2 in the pre-treatment condition (Figure 8). Additionally, the spatial arrangement of the post-treatment inundated area is so widely dispersed that wetted edge increases from approximately 5,559 m pre-restoration to over 32,000 m post-restoration. In terms of complexity, the pre-restoration wetted edge complexity index was 7.8 compared to a complexity of 23.1 in the post-restoration area.

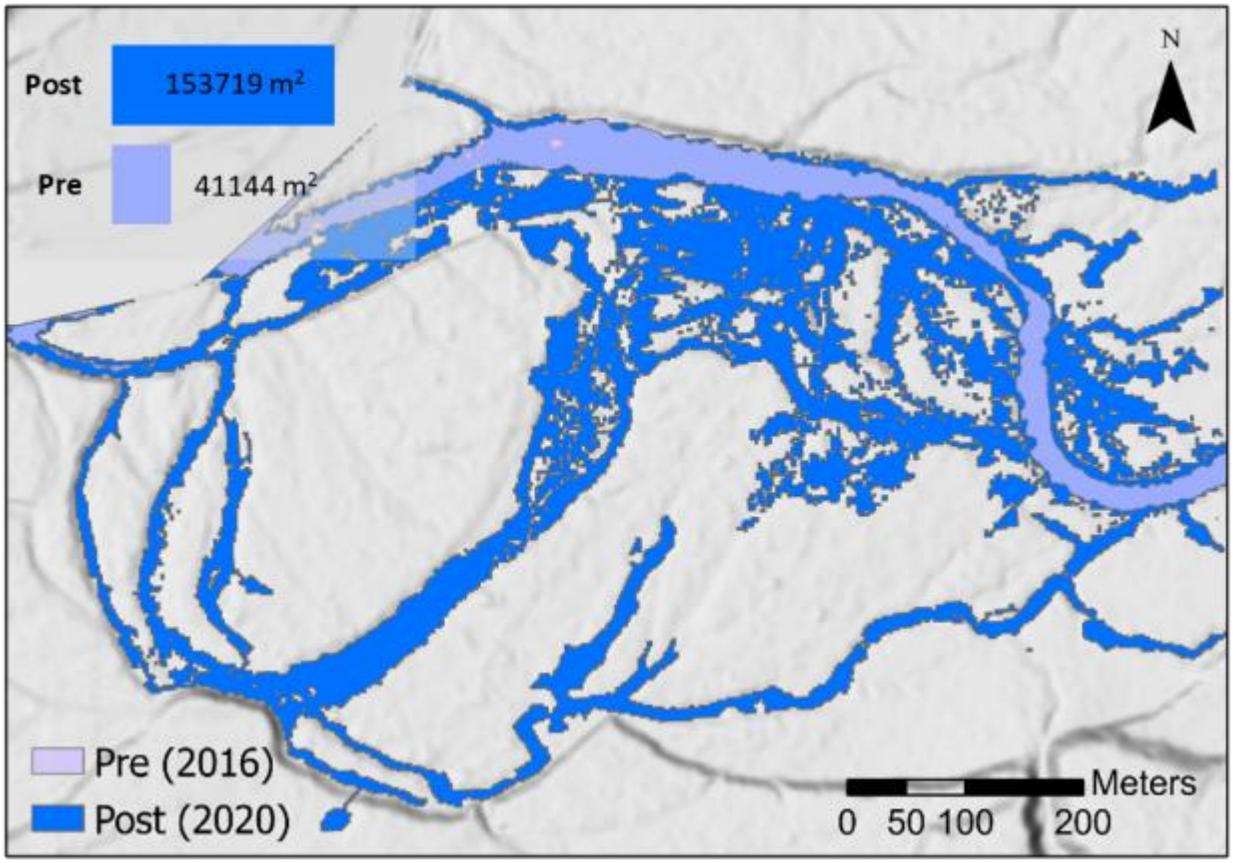

Figure 8: Pre- and post-treatment inundated area at within the Phase I restored reach at the South Fork McKenzie River.

Discussion – Inundated Area:

The NDVI calculated from the near infra-red sensor band in the UAS imagery effectively identified all visible water making it relatively easy to map the extent of the inundated area. Overhanging vegetation, emergent macrophytes, and floating or suspended logs, however, created substantial challenges in the post-restoration conditions. Prior to restoration, the site was dominated by a relatively deep, simple, single thread channel in which large wood was rare. While vegetation would have overhung from the stream banks, the amount of wetted edge was

small, relative to the inundated area, leading to relatively small errors in the estimate of the inundated area. The post-restoration condition was quite different. The patterns of inundation across the floodplain were quite complex, with many narrow channels, and tiny islands so that the wetted edge was large relative to the inundated area. Further, thousands of logs had been placed throughout the site. As a consequence, substantial portions of the inundated area, obvious to a field observer would be classified as "dry" if mapped solely on the basis of NDVI determined from the UAS imagery.

The resolution to this issue depends greatly on the topic area of interest. For example, these obscured areas would be important to include when estimating the area of aquatic habitat – perhaps doubly so as both vegetation and logs would provide hiding cover for aquatic organisms. In contrast, if the UAS imagery is being used to estimate surface water temperatures, then it would be critical to "mask-out" objects that obscure the visibility of the water surface. The temperature of these objects could be radically different than the water temperature, giving erroneous estimates of water temperature across the site. The difference between these two approaches to estimating inundated area is easily seen by comparing Figure 8 (above) with Figure 23 in the section on water temperature (below).

Large In-Stream Wood

(Reporting work led by Matthew Barker and Michael Wing, Oregon State University, College of Forestry, University Aerial Information Systems Laboratory)

Introduction – Large Wood:

Large in-stream wood is a critical components of fluvial systems that are associated with increased sediment deposition, greater complexity, increased heterogeneity of flow regimes, and it can provide high quality habitat for salmonids and other fishes (Sass 2009). Here, we used the US Forest Service Forest Inventory and Analysis (FIA) definition where large wood is downed pieces of wood with a small-end diameter of at least three inches and an overall length of at least three feet (Woodall and Williams 2005). One of the overall objectives of the South Fork McKenzie Stage-0 restoration are to retain 90% of the deposited wood for five years. This provided us with a unique opportunity to utilize imagery recorded with an unoccupied aircraft system (UAS) to quantify the amount of wood throughout the project site. In this project, we sought to pair object-based image analysis, machine learning, and classical sampling approaches to produce estimates of the target parameter, two-dimensional large wood area, throughout Phase 1 and their associated 95% confidence intervals.

Methods – Large Wood:

We acquired imagery covering ~60 hectares of Phase 1 on 23 September 2019 (Table 2) using the DJI Matrice 200 v2 with Micasense Altum multispectral sensor. Imagery was processed with Agisoft Metashape structure from motion software to produce a 6-band 6 cm GSD orthomosaic of the site (Figure 9). Then, we simplified the imagery by clustering similar pixels into image segments. These segments contained 40 summary statistics of the image properties including reflectance in the five electro-optical bands and radiant temperature in the thermal band as well as information such as segment area and roughness. We used these data to train a random forest classifier to detect large wood image segments (hereafter RF wood) in a 1.4-hectare subset of the site that contained features represented throughout Phase 1. We assessed the model performance and used the classifier to predict large wood throughout the site.

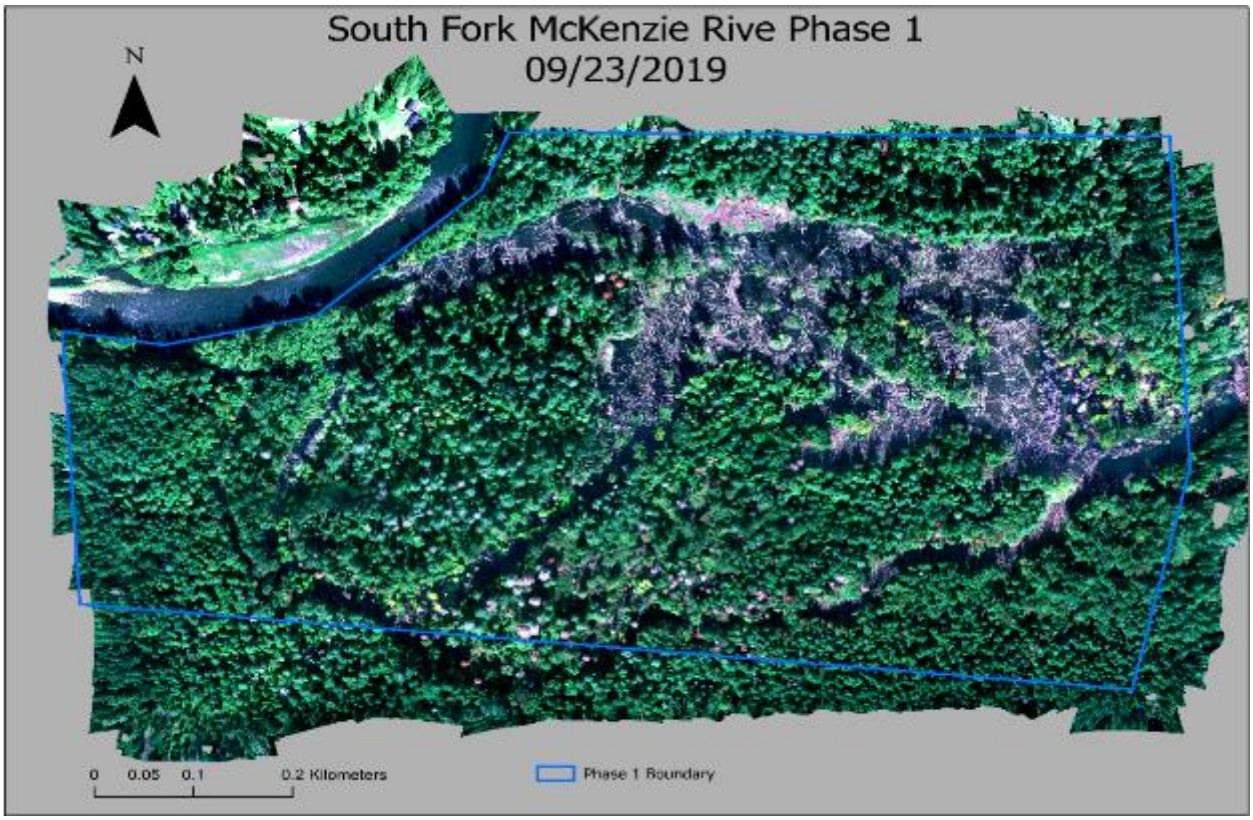

Figure 9: Phase 1, South Fork McKenzie River Orthomosaic

To sample the imagery, we generated 51.46 m^2 hexagons and classified them as forest, wetted, or barren. We removed the forested hexagons, leaving a population of N = 3,858 hexagons. We randomly sampled n = 40 hexagons (Figure 6) within which we located four 1.0 m radius subplots (Figure 7). We surveyed the subplots and estimated percent wood cover. Then, we manually delineated large wood in the 40 randomly sampled plots with GIS software, extracting auxiliary variables that included average reflectance in red, green, blue, rededge and near infrared, as well as average radiant temperature and the estimated large wood area from the random forest classifier. To ensure our manually delineated large wood was representative of ground condition, we employed Spearman's rank test to assess the correlation between manually delineated large wood and field estimates.

Last, we used four estimators to quantify two-dimensional wood area: simple random sample without replacement (SRSwoR; Thompson 2012), difference estimator (Godfrey et al. 1984), simple linear regression (SLR), and a general regression estimator with multiple auxiliary variables (GREG) (McConville et al. 2020).

Results and Discussion – Inundated Area:

The random forest classifier performed well in the training area with a kappa of 0.76 and balanced accuracy of 0.86. After removing occluded subplots, results of Spearman's rank test strongly suggest a non-0 correlation between our field estimates of large wood and GIS

delineated wood ($p < 0.001$, $\rho = 0.57$). The high ρ suggests that GIS manually delineated wood is a reasonable target parameter to estimate two-dimensional large wood area. After assessing the variance and producing 95% confidence intervals using the four estimators, we found SRSwoR resulted in the largest estimate for large wood area and widest confidence interval, whereas the GREG estimator resulted in the smallest estimate and narrowest confidence interval (Table 4). SRSwoR is the simplest estimator to implement and does not require data produced by the random forest classifier. However, there is less uncertainty associated with the more complex GREG estimator.

The wide confidence intervals are likely a due to the complex nature of the site with tree branches, gravel beds, and water obscuring and/or mixing with the wood, preventing the spectral classifier from identifying distinct *n*-dimensional spectral boundary associated large wood. The methods employed in this analysis are novel and the complexity and uncertainty are reflective of the developmental nature of this work. Despite the wide confidence intervals, these data provide a reference point for evaluating future change conditions. Additionally, the relative similarity of estimated large wood among approaches is likely evidence a central tendency. These data could provide useful insights in productivity assessments as they represent the best-available estimate of wood available to macroinvertebrates. Future work could improve the science around Stage-0 remote sensing monitoring with analysis of spatio-temporal trends in large wood and the incorporation of neural network classifiers (e.g. TensorFlow) to improve accuracy and narrow confidence intervals.

Table 4: Two-Dimensional Large Wood Estimates

Estimator	Estimate (m^2)	95% CI (m^2)	Aux variables
SRSwoR	17,283	10,613 – 23,952	Manually delineated wood
Difference Estimator	17,272	12,191 – 22,353	RF wood
SLR	17,269	13,219 – 21,318	RF wood
GREG	16,593	13,054 – 20,133	Avgs: r, g, b, re, nir, lwir RF wood

Sediment

Introduction – Sediment

Sediment size distribution is a geomorphic attribute of streambeds associated with suitability of spawning habitat for salmonids. The pre-restoration stream bed was described as heavily armored and dominated by sediment classified as boulders and large cobble, which is corroborated by imagery taken of a undisturbed section of the river that was visible when flows through the channel were diverted during restoration treatment on Phase 1 (Figure 10). Restoration was expected to alter this condition substantially due to the bulldozing of material from the surrounding floodplain to increase the elevation of the historic river channel.

Conventionally, sediment size distributions are measured with field-based gravelometers or sieving methods using transects perpendicular to the stream and would provide some information about overall sediment size class distribution of in post-restoration SFMR. However, given the complex flow paths on the post-restoration site and the sheer size of the restoration area, we felt that such methods would be inadequate for characterizing the sediment size distribution across space and would thus be insensitive to detecting long-term changes. Additionally, post-disturbance sites are generally fragile from a biological perspective as the ecosystem must restructure around the altered physiographic conditions. As such our intent was to examine the efficacy and feasibility of using UAS to conduct sediment size distributions using photogrammetric principles in effort to address the two limitations of conventional methods expressed above. Additionally, there were concerns that site access would become increasingly dangerous with time due to changes in sediment depositional patterns, coarse woody material decomposition, and other in-stream hazards.

Figure 10: Pre-restoration Stream Bed Sediment - Image taken 1 July 2018 on an undisturbed reach during active restoration treatment when flow was diverted

The objective of this work was to (1) examine the efficacy of using UAS remote sensing for assessing sediment size distribution across space and time, (2) establish a baseline of sediment size distribution to facilitate subsequent temporal change analysis, and (3) determine if there is any evidence of sediment size distribution change between 2019 and 2020. Note that although data was available for 2021, funding limitations prohibited a comprehensive change analysis incorporating the 2021 data.

Methods – Sediment

Field measurement of sediment was described above (see section titled *Short-term changes on field validation plots*). Coincident to the field validation survey were 40 video/photo plot surveys with the Phantom 4 UAS, using the methods also described above (see section titled *Aerial Survey with Unoccupied Aircraft Systems*). The distribution of the 40 plots was expected to capture variation of sediment size. The intent of the field validation surveys was to provide a corroborating account of sediment size distribution within each photo plot. However, due to positioning imprecision of both the UAS, and the validation plot center, photo plots were not well aligned with the field validation plots. Additionally, subplots were not included in the analysis if less than 50% of the plot area was on the flood plain and exhibited no evidence of scour. As such, for the 2019 and 2020 surveys, only a small subset of photo plots was usable for sediment analysis (Table 5). Note that comparisons back to the pre-restoration condition were not possible because deep water in the narrow, single-thread channel obscured visibility of streambed, even during summer low flows.

Table 5: BASEGRAIN Results for 2019 and 2020. Plot indicates the plot ID associated with data. Median (mm) is median sediment size for that plot. Area * b is a BASEGRAIN output (drop if it doesn't show a relationship with field median). Field median (mm) is the median sediment size as measured by the gravelometer across all four sub-plots.

2019		
Plot	median (mm)	Field Median (mm)
8	28.2	68.2
9	45.6	83.3
19	30.7	48.5
26	23.6	26.6
35	16.7	-
Mean	29.0	56.7

2020		
Plot	median (mm)	Field Median (mm)
8	55.2	50.0
-	-	-
19	16.3	34.2
-	-	-
35	27.6	26.9
Mean	33.0	37.0

Photo Plot Processing

Photo plots were processed with the BASEGRAIN ver 2.2 (Detert and Weitbrecht 2013). BASEGRAIN is a granulometric analysis (i.e., photosieving) software that conducts object base image analysis methods to segment nadir pointing imagery (i.e., top-down view) to detect individual sediment grains, estimate an *a* and *b* axis lengths and produce a quasi-sediment size

distribution that are comparable to estimates generated from hand-held USGS US SAH-97 analyzer (Wolman 1954).

Each photo plot image was first oriented such that image top is north by overlaying the image on an orthomosaic of the site in ArcGIS Pro and conducting a rigid transformation (translation and rotation) using manually identified key points. This produced an estimated GSD and oriented the images. Scale across the image is assumed to be homogeneous due to radial distortion lens correction profile that is automatically applied to the image at the time of creation and minimizing the likelihood of a non-orthogonal image capture by having the camera mounted on a three-axis stabilized gimbal that is pointing nadir (i.e., camera sensor plane is parallel to earth surface). We also had precise altitude information with which to scale the imagery in terms of mm/image pixel via the laser altimeter described previously, however, due to the need to orient the images to north, it was simpler to simply conduct a rigid transformation as described, than to estimate GSD with the laser altimeter.

BASEGRAIN:

BASEGRAIN processing was a four-step process whereby the photo plot image was loaded into ArcGIS Pro (Fig 11a), and subplots described in previously (Fig 7a) were clipped out of the image (Fig 11b). Each clipped image was individually processed in BASEGRAIN to segment the sediment from the image (Fig 11d) and produce a sediment size distribution (not shown). Processing followed the workflow described in section 4 of Detert and Weitbrecht (2013).

Results – Sediment

Due to the relatively sparse nature of the dataset, the data provide minimal inferential capability for drawing conclusions about conditions of the entire site with only a year's change between surveys. However, the paired nature of the UAS and field plot data in in 2019 and 2020 facilitate a cursory examination of relationships and trends.

No obvious correlation between UAS and field data was present. In some instances, field estimates were greater than UAS estimates, and vice versa. Furthermore, the amount of person on keyboard time to get to this relatively coarse summary was extensive when accounting for pre-processing, and analysis, the estimate is upwards of 50 hours. Examination of the BASEGRAIN image outputs suggest that in many plots the data exhibited over segmentation where large sediment clasts were incorrectly split into multiple smaller sediment classes by the software.

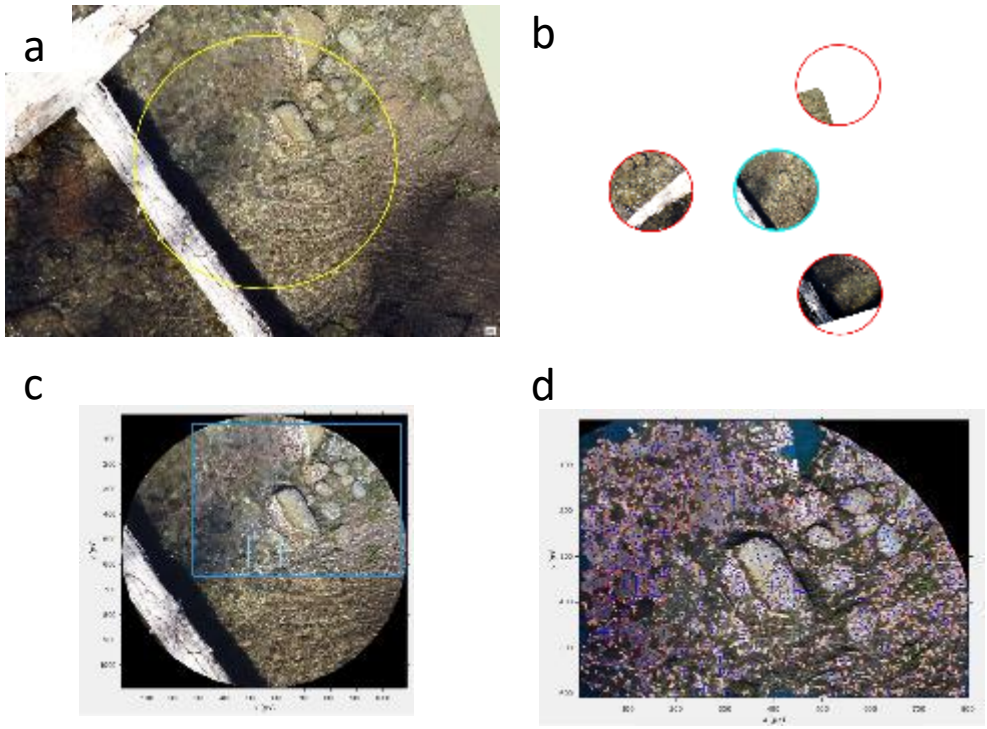

Figure 11: BASEGRAIN Process - a) raw photo plot image, b) clip outsubplot imagery (see Fig 7a), c) process each subplot image through BASEGRAIN; note this figure is from the center subplot in b, d) segmented image from BASEGRAIN.

Discussion – Sediment

The limited amount of data prohibited a thorough analysis, which speaks to the inefficiency of implementing the method as presented here. The ineffectiveness was partially due to the inability to control environmental conditions that create shadows and wet (dark) areas on the sediment surface, which are both conditions in which BASEGRAIN is known to over segment (i.e., break a single large clast into 2 or more smaller clasts). It is unclear how over segmentation will affect the estimated size distribution of the streambed sediment. Clearly, by breaking large clasts into two or more smaller clasts, the BASEGRAIN analysis must underrepresent sizes of sediment particles. This was clearly seen in the estimated median diameter of the sediment from the 2019 plots whereas the median diameters are in much closer agreement in the 2020 plots. Note, however, that the median is only a single metric and may not capture other differences in the sediment size-class distributions.

The authors of the BASEGRAIN software have recently released a compendium of case studies and techniques for using BASEGRAIN in non-optimal conditions that if implemented, may improve results of future analyses (Detert and Weitbrect 2020). However, the sampling methods, using relatively small 1-m radius sub plots, and the relatively poor GNSS accuracy prohibited good alignment between field and UAS data. We recommend that future uses isolate

sediment imaging to areas of the channel that are inundated during high flow, but dry in low flow, then supplement with field gravelometer measurements along transects of the wetted channel. While it may be potentially attractive to focus sampling on areas exhibiting deposition and scour, we caution that such an approach, while informative to changing conditions, may impose bias on the measurements and not adequately characterize habitat quality from a biological perspective.

From a technical perspective, the method would benefit from more precise georeferencing of the field plots and the UAS locations. The RTK capable UASs that are now more widely available would help solve this problem. Also, field survey plots should also be georeferenced and plot centers (or corners) clearly flagged with a large target (~25 x 25 cm) of contrasting color to enable the pilot to more reliably identify the plot center. Furthermore, limiting aerial surveys to times with complete cloud cover would likely reduce over segmentation, a position that is supported in the BASEGRAIN manual. There's also the potential that other image analysis methods such as Convolutional Neural Networks, SediNet, or DigitalGrainSize are better suited for the task, however, due to limited funding we were unable to explore these options (Buscombe 2013; Rains 2019; Buscombe 2020; Lang et al. 2021; Chen and Fu 2022).

Conclusion – Sediment

The UAS granulometric analysis as implemented here leaves substantial room for improvement. Considering the pilot time spent flying photoplots and analyst time spent processing and analyzing the data, the UAS granulometric analysis did not exhibit improved efficacy over conventional field methods as currently implemented. It did, however, demonstrate the improved personnel safety of using remote sensing approaches, which are of ever-increasing concern on the site as coarse woody material degrades and vegetation recruitment increases, increasing the risk associated with field work.

Flow velocity

Introduction – Velocimetry

Understanding stream velocity is often an objective of salmon habitat suitability but is also a characteristic that is important to other biotic components of stream systems as well as the hydrologic and geomorphic aspects of streams (Rosenfeld, 2011). Typically instream velocity is measured at a fixed gaging station or via relatively sparse in-situ measurements made with instruments such as a velocimeter or flow meter along lateral transects across the stream. In single-threaded channels where dominant flow direction and velocity is generally consistent, sparse measures of velocity are likely to be more representative of overall stream condition and informative to understanding velocity influences on abiotic and biotic components of the stream. In a complex reach like the post-restoration SFMR Phase 1 where channel depth is highly variable, large instream wood is interspersed throughout the inundated area and flow is dispersed across a broad expanse of stream bed, relatively sparse measures of stream velocity are not likely to be informative to understanding velocity influences on abiotic and biotic processes and functions.

Emerging technological advances in the field of image processing have produced algorithms for Large Scale Particle Image Velocity (LSPIV). The LSPIV algorithms examine surface texture in videos of streamflow and extract estimates of flow velocity, flow direction, and flow vorticity (Sutarto, 2015), and have been shown to be accurate in controlled conditions, such as measuring velocity and discharge through experimental flumes with known channel geometry. Pairing UAS with LSPIV offers the opportunity to measure stream velocity in more complex, less structured settings and previous work has shown that velocity estimates are relatively accurate (Tauro et al., 2016; Lewis et al., 2018). However, there are known limitations with LSPIV when tracers (i.e., patterns in the water surface indicative of velocity and flow path) are not evident and when the imaging system is unstable.

Here we examine the efficacy of using UAS and LSPIV to conduct velocimetry measurements to produce estimates of surface flow velocity, vorticity, and direction in the post-restored Phase I area of SFMR. We compare UAS estimates to field estimates where paired data are available, summarize UAS estimates, and provide estimates on processing time to provide perspective to future adopters of this technology with a sense of the barrier to entry.

Methods – Velocimetry

Field measurements and UAS surveys:

Field measurement of water flow velocity was described above (see the section titled *Short-term changes on field validation plots*), and was collected at 39, 23, and 15 plots in 2019, 2020, and 2021, respectively. The number of field plots measured in 2020 and 2021 resulted from the combined effects of the COVID pandemic and the Holiday Farm fire. UAS video/photo surveys were collected at the same time with the Phantom 4 UAS, using the methods described above (see the section titled *Aerial Survey with Unoccupied Aircraft Systems*). The distribution of the plots was expected to capture variation of surface velocity. The intent of the field validation

surveys was to provide a corroborating account of velocity distribution within each photo/video plot. However, due to positioning imprecision in of both the UAS, and the validation plot center, photo plots were not well aligned with the field validation plots, reducing paired field and UAS observations within years, and pairings of UAS observations among years. Additionally, subplots were not included in the analysis if less than 50% of the plot area did not contain water. As such, UAS processing was limited to the six photo/video plots having the best year-to-year overlap. Unfortunately, those did not align well with field plot measurements collected in 2020 and 2021, resulting in 5, 2, and 2 paired comparisons between UAS and field observations, in 2019, 2020 and 2021, respectively.

Processing

Video data from 2019, 2020, and 2021 were processed for plots 7, 8, 9, 19, 23, and 35. Processing was performed using the Rectification of Image Velocity Results (RIVeR; Patalano et al., 2017) and Particle Image Velocimetry (PIV; Thielicke and Sonntag, 2021) applications in Matlab (Mathworks 2014). RIVeR is an open-source version of PIV, which is an implementation of LSPIV described earlier and was only used to import 10 seconds of imagery from each video survey. Analyst discretion was used to determine the optimal 10 second segment to extract. Since the videos were 4K resolution collected at 30 frames per second, this resulted in 240 frames for evaluating LSPIV. Extracted frames were cropped and corrected using a video stabilization script to reduce the influence of sensor and aircraft movement on LSPIV estimates (Engel 2020, Farid and Woodward, 2007). Stabilized video frames were processed in the PIV software to produce LSPIV metrics. Prior to running PIV, the analyst first cutout areas in the video frames that might confound results such non-water areas (i.e. ground, logs, leaves), clear slack water and shadows (Figure 12a). Additionally, video frames were scaled to linear metric units using known intrinsic parameters of the video sensor and the sensor height above water as estimated by the laser altimeter. Scaling allows PIV to output results in metric units instead of pixel-space units. For time between frames, we used 1/30 s, because the sensor was programmed to record at that rate. Due to altimeter data being unavailable for 6 plots in 2019, and 2020), these photo/video plots were not included in this analysis. Results were saved into an ASCII file of LSPIV metrics. An image of the velocity direction vectors is shown in Figure 12c.

ASCII files were imported into R for follow-on analysis. Follow involved estimating LSPIV processing area (m^2) for each plot and year, estimating 2.5, 50, and 97.5 percentile velocity magnitude, velocity direction, and vorticity estimates. Quantiles were chosen to facilitate rapid comparison to field data due to the different data densities. Velocity direction estimates first corrected to match compass orientation from the -/+ 180° polar coordinate system generated in PIV for the purpose of producing an azimuthal interpretation. We then used the $atan^2$ of sine and cosine of quantiles of velocity direction measurements in units of radians, which is a common method for estimating central tendency of unit circle data to prevent the artificial boundary between 0° and 360° from influencing estimates. Field estimates of surface and 60% water depth velocity were also compared to UAS LSPIV estimates. We also provide processing times to provide future users with a sense of the tradeoff for field time and computer time.

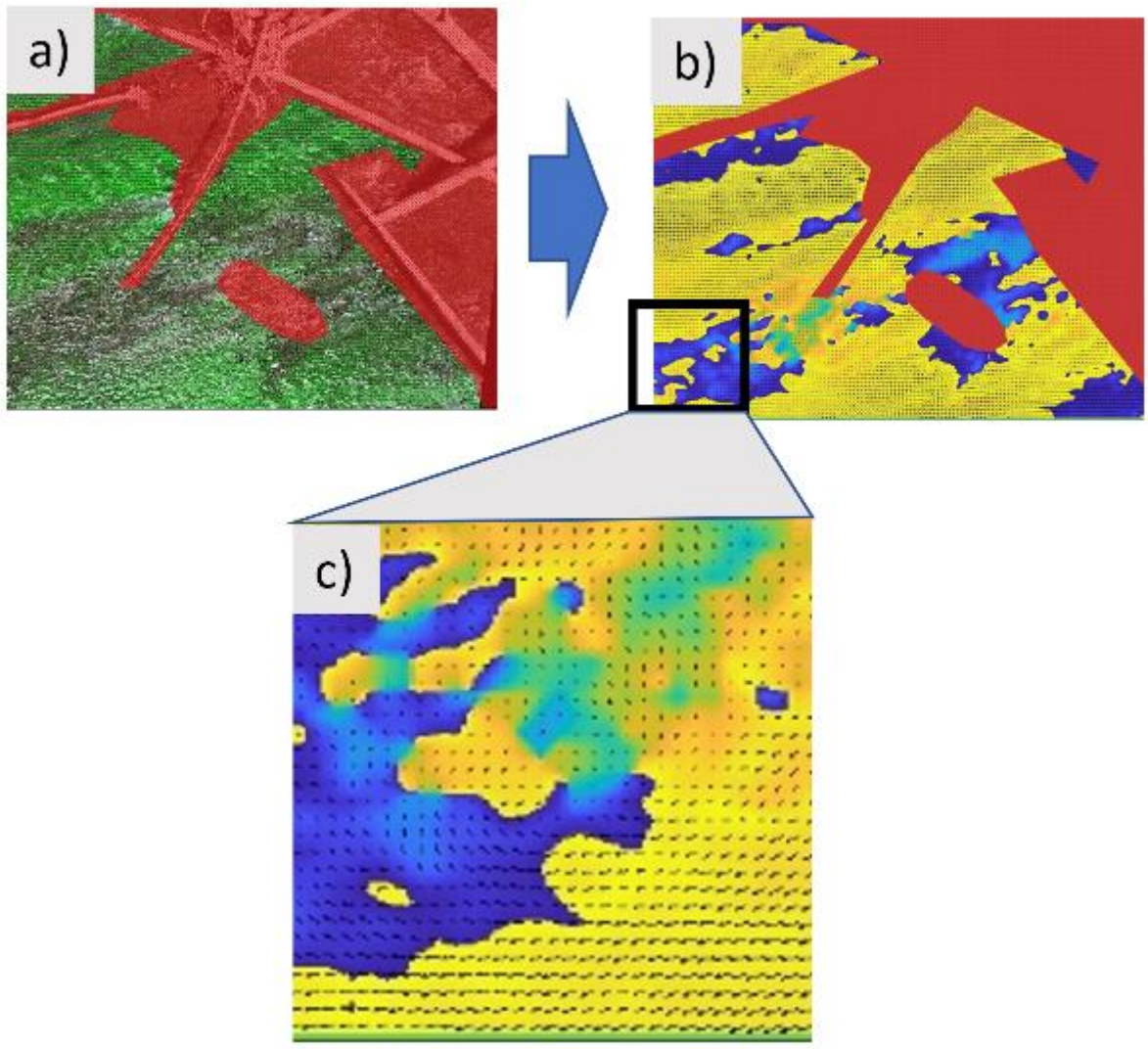

Figure 12: PIV processing example. a) masking (red-shade) non-water from video frame, b) estimating the velocity and direction vectors for each video pixel, c) zoom in of PIV output depicting direction vectors over relative velocity.

Results – Velocimetry

Processing time. Total time for processing the nine video plots presented here was 35 hours of analyst time plus 18 computer hours running RIVeR and PIV. Note that analyst times includes the time it took to develop and refine the processing method.

Due to variation associated with the process of masking potentially problematic areas from video frames and the variation of UAS positioning over repeat measurements, total processing area for each plot varied significantly (Figure 13). Note that the target was 52 m^2, which corresponds with the overall area of each plot in the tessellation grid described earlier.

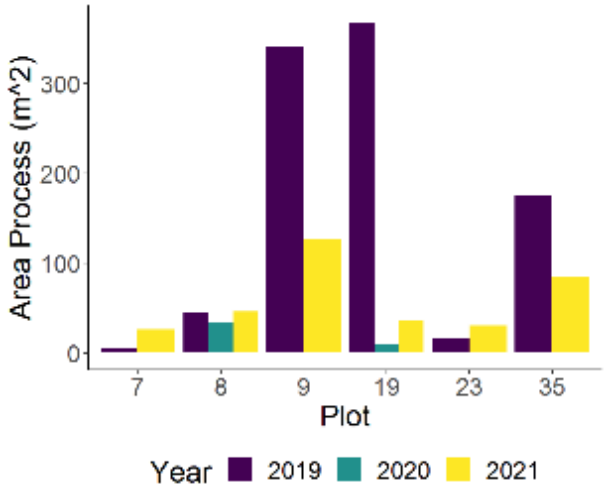

Figure 13: UAS LSPIV processing area by plot for each year.

Repeat measurements of velocity by plot for each of the three years exhibit significant variation (Figure 14a and Figure 14b).

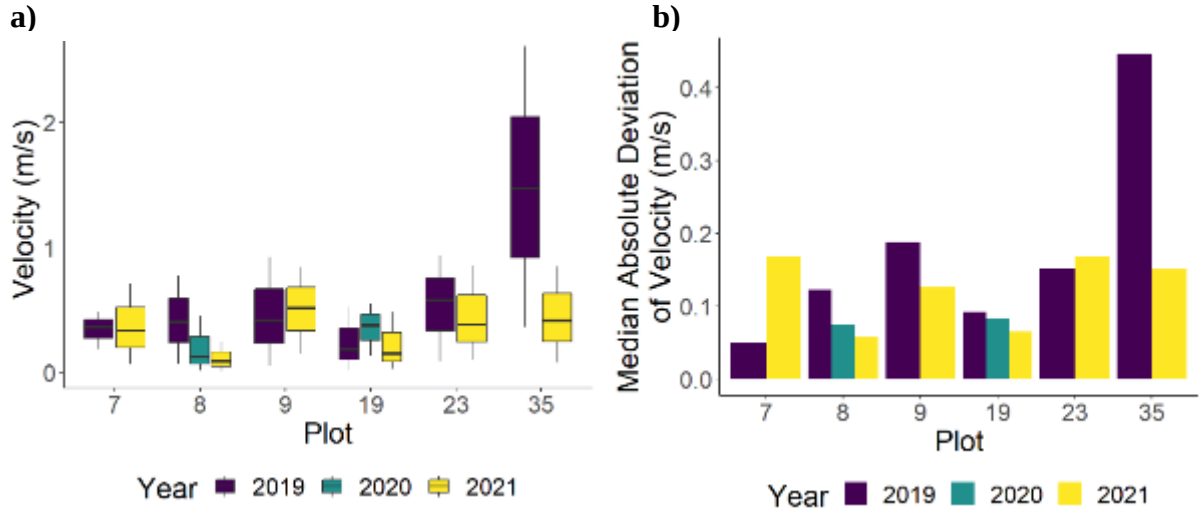

Figure 14: UAS LSPIV Velocimetry. a) boxplots representing 95% of the distribution of estimated velocity by plot and color by year. b) Mean absolute deviation of estimated velocity by plot and colored by year.

Flow direction estimates exhibit substantial differences between plots as well as high levels of variation within plots some years and exhibits an overall west southwesterly flow direction (Figure 15a). Median Absolute Deviation does not appear to exhibit strong correlation with the total area being analyzed (Figure 15b; Figure13), which may indicate that very large plot sizes are not necessary to capture heterogeneity in the velocity distribution.

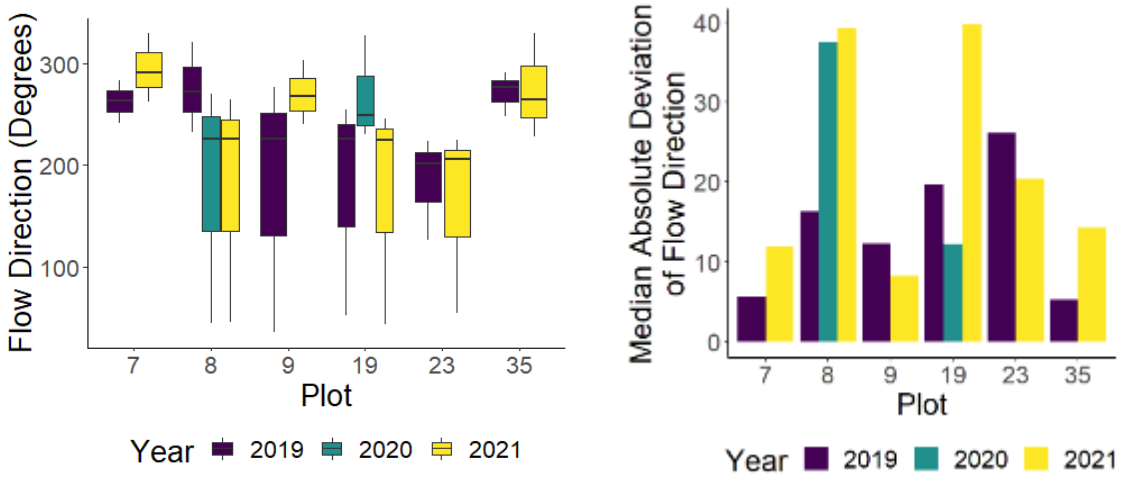

Figure 15: Flow Direction - a) Distribution of flow directions by plot and year, b) median absolute deviation of flow direction by plot and year estimated from the UAS LSPIV method

Comparisons of UAS velocimetry estimates compare closely in plot 9 in 2019, plot 8 in 2020, and in both plot 19 and 35 in 2021 (Figure 16a). UAS estimates of MAD indicate the UAS velocimetry is more variable than the field measures (Figure 16b).

Spatially explicit examinations of change using the UAS data were not feasible due to the significant variations in processing area form plot to plot and from year to year. Similarly, single-point field measures are not directly comparable among years because observation locations were in the vicinity of the specific subplot, but not always in the same location each year.

Discussion – Velocimetry

The UAS LSPIV velocimetry present compelling results with velocity distributions that, while generally higher in velocity than the field data, overlap in agreement. Given the relatively low sample size these results must be treated with caution, but the general agreement provides evidence supporting the concept. A more comprehensive comparison between field and UAS LSPIV estimates is strongly recommended. It should be noted that these flow direction analyses are based on relatively small spatial extents, less than 8 m^2 in some cases. Additionally, logs, boulders and gravel bars alter flow significantly at the scale of this analysis, further confounding the ability to discern a global velocity trend from relatively small plots. Note that the pilot was instructed to conduct these photo/video plot surveys such that the top of the camera was always oriented north, so the rotation correction was not due to camera orientation.

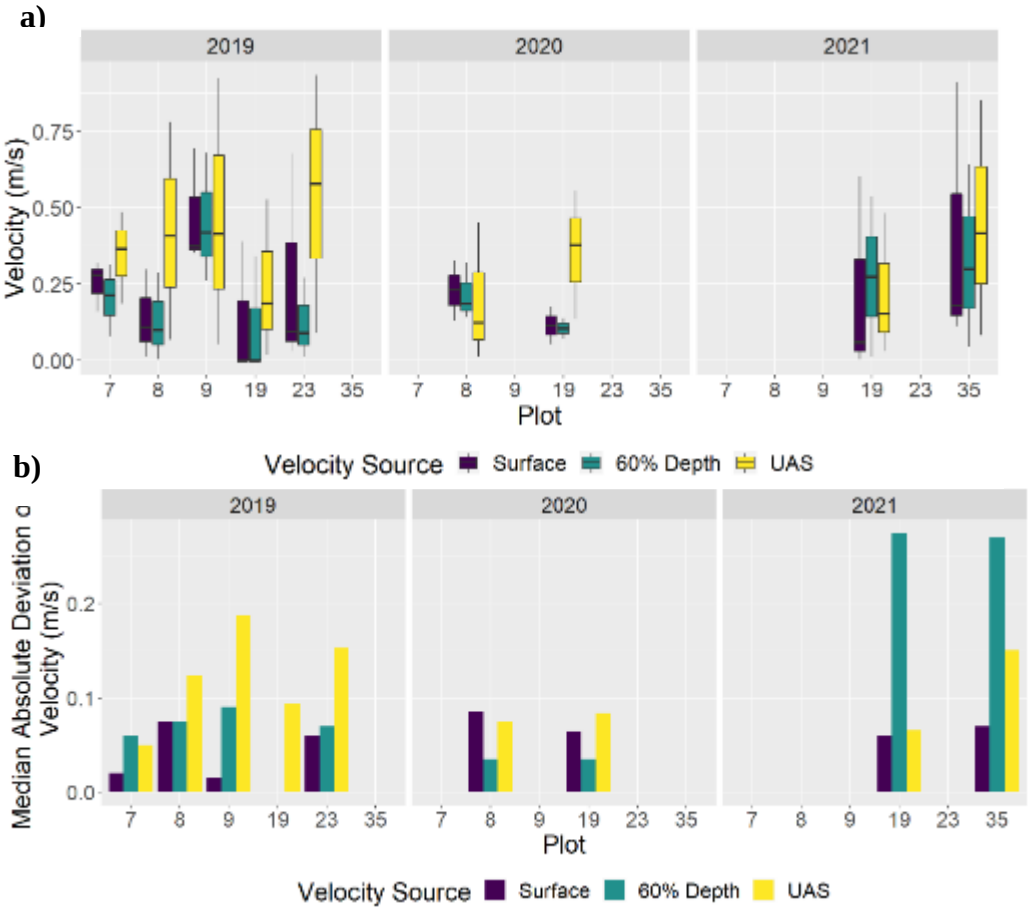

Figure 16: Comparison of Field Measurements to UAS - a) velocity comparison among two field measures (surface velocity and velocity at 60% depth using a flowmeter) and UAS for each plot and year. b) Estimate of median absolute deviance among the velocity observation sources by plot and year.

It was not possible to conclusively determine if median velocity and direction changed over time due to the limited sample size. This is further confounded by the fact that overall water moving through the channel system was progressively less for each of the three survey periods as evidenced by the Rainbow gauging station discharge history (Table 2).

There are several limitations imposed by the method as implemented here. The two largest limitations were, 1) the time costs associated with flying and subsequently processing the data, and 2) the poor plot referencing. The time cost would likely reduce as analysts and pilots become familiar with the process. To improve image georeferencing efficiency, we recommend either using a UAS capable of precise navigation with Real-Time Kinematic (RTK) positioning, or the installation of in-stream reference monuments that are visible to the pilot via the real-time video feed. Improved referencing would ensure more consistency of the processed area for repeat measurements and ensure alignment with field observations. Other issues were that the photo/video plot sample size was intended to be 120 plots but was cut to 40 plots to reduce costs associated with data collection and processing. Imaging 120 plots would have likely taken three days of UAS survey time (in the field), and based on our work here, about 240 hours to process.

The UAS LSPIV approach could capture the full range of surface velocity conditions over a large area with a surprisingly fine-grain, resulting in a detailed dataset quite different than the sparse sets of field-based observations more commonly collected. However, extracting the velocity fields requires about 1.7 hours of analyst time and 2 hours of computer time per plot. Thus, capturing a broader more comprehensive network of plots than we've reported here would result in substantial costs.

The UAS LSPIV method produces thousands of velocity data points per plot, which makes it very efficient from a data density (data points per unit of area) standpoint. And while we understand that aquatic species live in and respond to these complex velocity fields, this sort of detailed information has never before been readily available. Thus, the tools needed to interpret these fine-grained velocity fields in a biologically meaningful way have not yet been developed. Thus, the UAS LSPIV approach offers an interesting opportunity, but one that awaits development of specific applications.

Conclusion – Velocimetry

The results of the velocimetry analysis suggest there is merit in exploring UAS LSPIV for operational implementation in stream conditions where the technological overhead represents an increased efficiency over conventional in-stream methods. We present evidence that suggests the UAS + LSPIV method more comprehensively captures the complex stream flow conditions at SFMR following restoration treatment. However, future implementations of the method presented here should use a sample design not dependent on repeat observations of specific locations in space or should include efforts to ensure the UAS video captures roughly the same footprint each year. Additional work is necessary to realize the full value of the LSPIV UAS data and how it might be used in habitat suitability models or sediment transport and deposition models. Nevertheless, our experience here suggests that the UAS LSPIV approach represents an interesting opportunity awaiting further development.

Stream Temperature:

Introduction – Stream Temperature:

The multi-spectral sensor that we used in most of our UAS surveys included a thermal infrared sensor that recorded surface temperatures of objects viewed by the sensor. The sensor also recorded the near infrared which can be used to distinguished between water and other surfaces. Thus, the thermal imagery could be used to estimate the water surface temperature across the entire inundated area of the 0.97 km long restored reach. As part of our efforts toward methods development, we decided to instrument the restored reach with a number of recording temperature data loggers which could provide the necessary validation data to test the accuracy and precision of the thermal infrared band from the multi-spectral sensor.

Discharge and water temperatures of the SFMR are highly regulated below Cougar Dam. Obviously, the dam regulates river discharge, but the intake tower was retrofit in the early 2000s by building "*adjustable weir gates*… [that] …*allow dam operators to selectively draw water from various depths of the reservoir and mix it to a temperature more closely matching pre-dam downriver conditions*"[2]. Thus, both flow and temperature can be regulated through dam operations. The restoration of significant lengths of the riverbed and valley floor to a Stage-0 condition (Cluer and Thorne, 2014) increased the exposure of the river water to direct solar radiation and should increase the river temperature. Because we collected data relevant to this question, we conducted an *a-posteriori* examination of these data to illuminate potential influences of the restoration on the stream temperature regime.

Methods – Stream Temperature:

Thirty-four HOBO U22 temperature data loggers were deployed in early August 2019, before a planned UAS flight, and retrieved some weeks later (Figures 17 and 18). All loggers were in place for a 42-day period, from 13 August through 22 September 2019. Loggers were programmed to record instantaneous temperature every 30 minutes. They were anchored in place and shielded from direct sunlight using a length of PVC pipe. The accuracy of each logger was tested against a NIST traceable reference thermometer (#B7117065) before deployment in 2019 and again after deployment in 2021. On average, the U22s showed a positive temperature bias of 0.016 °C and the largest errors in any instantaneous point measurement for any logger were -0.14 and +0.17 °C.

Not all of the U22s were relocated and retrieved in September 2019, and a few more U22s were redeployed in October 2019, including one newly deployed logger located at the Forest Road 19 (FR19) bridge over the SFMR, approximately halfway between the USGS gage and the middle of the Phase 1 restoration reach. These 7 loggers were in place from fall 2019 through at least late summer 2021. The difference in temperatures between the USGS gage and FR19, divided by the length of channel between these two locations, provided an estimate of the rate of heating for every 30-minute observation. Knowing the rate of heating (or cooling), and the

[2] From the US Army Corps of Engineers web site: https://www.nwp.usace.army.mil/Locations/Willamette-Valley/Cougar/ accessed on 22/02/2022.

distance between FR19 and the middle of the Phase 1 restoration reach, allowed us to estimate the expected pre-restoration temperature of the SFMR in the restored reach. We did not observe any substantial difference in the timing of daily maximum temperatures in these two locations and therefore did not build a time lag into our calculations of the expected pre-restoration temperature.

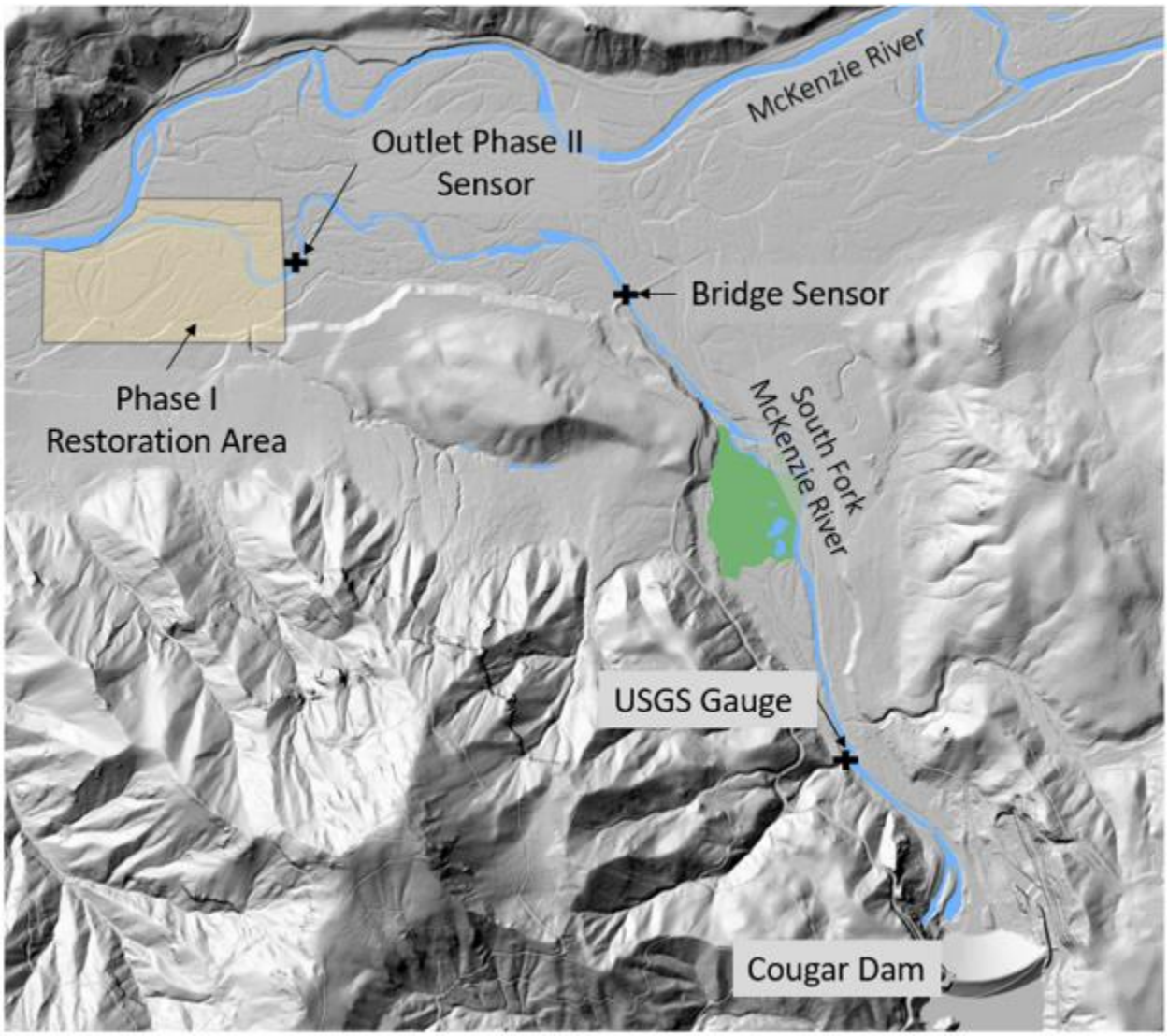

Figure 17: Location of Phase I restoration area shown in Figure 18, along with locations of sensors located at the top of the Phase I restored reach, at the Forest Road 19 bridge, and at the USGS gaging station below Cougar Reservoir.

Thermal imagery was also collected during each UAS survey. Here, we illustrate the results of those aerial surveys with imagery collected on 4 September 2020 between 20:46-22:18 UTC (1:46 to 3:18 PM PDT or local time). Individual thermal images were mosaiced using Metashape (version 1.4, Agisoft LLC, Petersburg, Russia) to produce a single 101 cm ground sampling distance (GSD) orthomosaic of estimated surface temperature. The inundated area, derived from the near infrared imagery collected during the flight, was used to mask out non-wetted areas and

thus isolate surface temperature grid cells corresponding to water. Temperature was not adjusted to account for local atmospheric conditions. Further, the thermal imagery is limited by the fact that it is more representative of surface temperatures than temperature at depth, unless the water is well mixed. We plan to continue developing and testing the UAS-based water temperature methods, but, as of yet we have not validated the thermal imagery. The temperature data derived from the thermal imagery and reported here should be interpreted with caution. We note, however, that the sensor is factory calibrated to have a linear response to temperature, so relative differences in temperature are expected to be representative of actual conditions assuming atmospheric conditions are homogenous across the surveyed area.

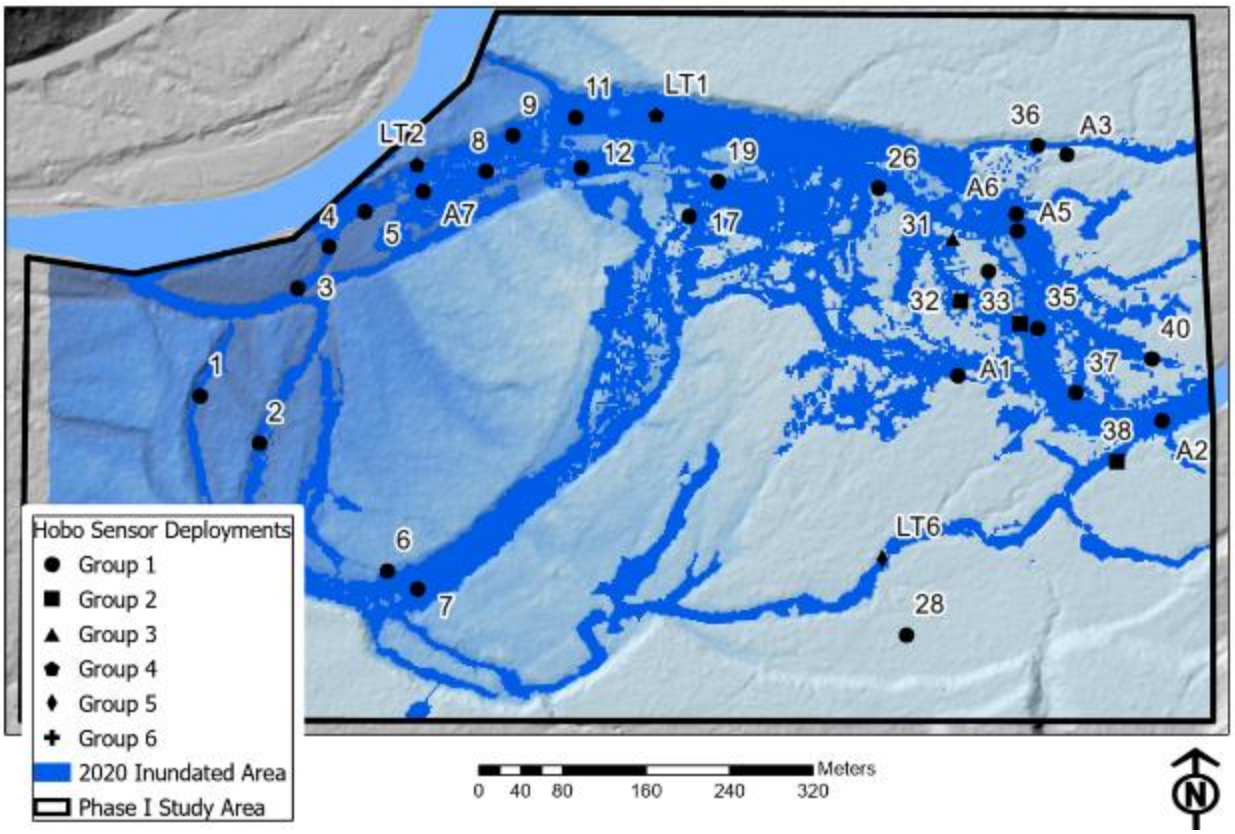

Figure 18: Location of individual temperature sensors within the Phase I restoration area shown in Figure 17. Labels conform to the Site IDs used to identify sensor locations in the database archived through Oregon DEQ. Symbols indicate the deployment period: Group 1 (circles) – August-September 2019; etc.

Because pre-restoration thermal imagery was not available, we are unable to conduct pre- versus post-treatment comparisons. However, the imagery from September 2020 covers a small portion of the main stem of the McKenzie River. The SFMR and mainstem McKenzie Rivers are not directly comparable. The mainstem temperature is greatly influenced by gold groundwater inputs from the high Cascade's aquifers and has higher discharge than the SRMR. However, the spatial heterogeneity in the water surface temperatures might reasonably represent the pre-restoration spatial heterogeneity of the SFMR because both channels are single threaded with armored, cobble and boulder dominated streambeds. Therefore, distributions of surface temperatures of the wetted area of the mainstem were compared to the surface temperatures of

the wetted area of the Phase 1 restored reach. Data were analyzed in R to produce summary statistics, and a Kalmogorov-Smirnov test was conducted to determine if the distribution of surface temperatures in the mainstem are different than the distribution in the Phase 1 project area.

Results – Stream Temperature:

The dam operations at Cougar Reservoir have a significant influence on the temperatures of the SFMR within our restoration reach. These influences are both direct and indirect. For example, the broad cooling trend from late August through early September 2019 (Figure 19) occurred without a significant change in discharge and during a period when air temperatures were relatively constant or increasing. Similarly, the abrupt cooling of the SFMR water temperatures, down to ~6 °C on 6 August 2020 occurred without a change in discharge or air temperature (Figure 20). Thus, these changes in stream temperatures result from the release of water mixed from different depths within the reservoir. Changes in discharge also influence the thermal regime of the SFMR. For example, on 24 July 2020, discharge increased from approximately 6 m^3/s to 17 m^3/s. This change in discharge led to a collapse in the amplitude of the diel variations in stream temperature within the restored reach despite little change in the temperature of water at the USGS gage immediately below the dam and little change in air temperatures. With little apparent change in the daily heat budget, the energy available to warm the stream during the day needed to warm nearly 3 times as much water and consequently the daily maximum temperatures decreased.

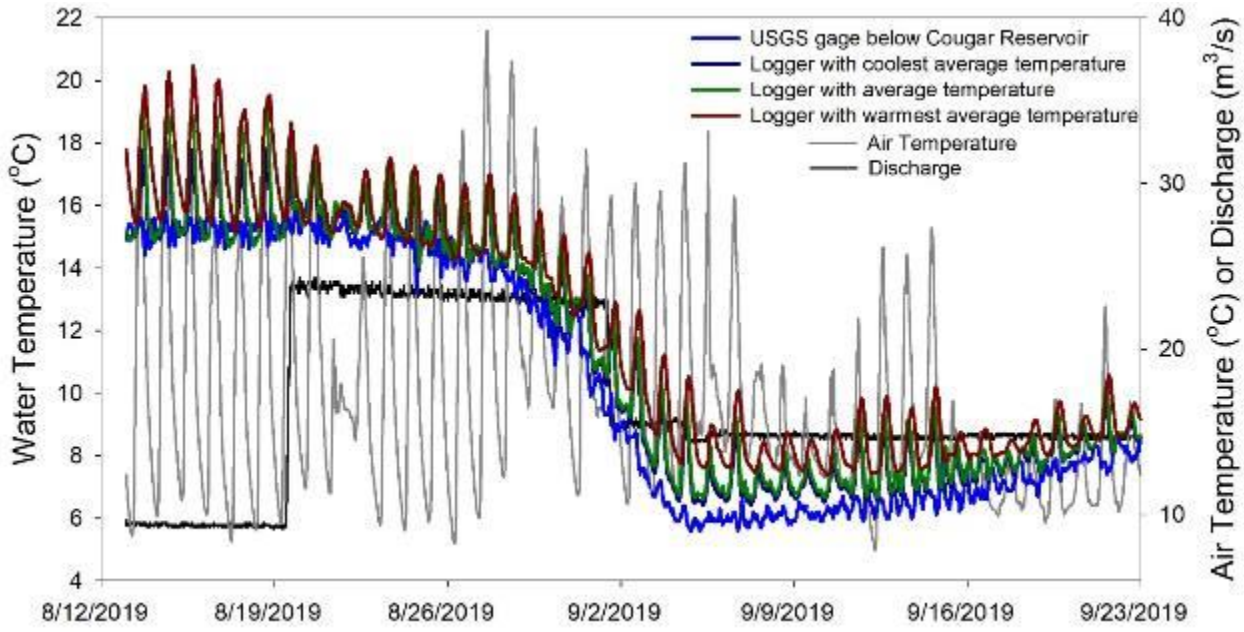

Figure 19: Time series of stream temperatures measured at the USGS stream gage immediately below Cougar Reservoir, and from the warmest, the coolest, and a near-average temperature data logger located in the Phase I restoration reach, located ~5.5 km downstream of the USGS gage. Also plotted are hourly air temperatures recorded from the PRIMET weather station, located at the H. J. Andrews Experimental Forest,

some 6.4 km away and 350 m higher in elevation as well as discharge measured at the USGS gage (#14159500).

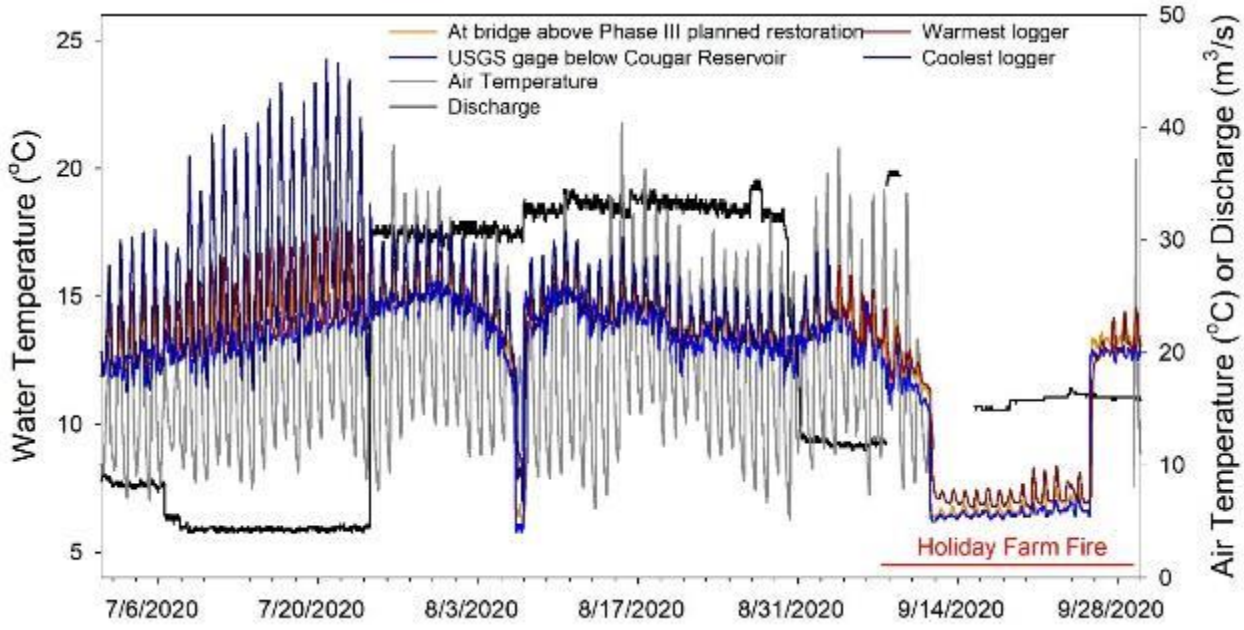

Figure 20: Time series of stream temperatures in the South Fork McKenzie River. Caption as in Figure 19, except temperature data are also shown for a logger located at the Forest Road 19 bridge over the South Fork some 2.8 km below the USGS gage and 2.3 km above the top of the Phase I restoration reach. Observations were made from midnight 1 July 2020 through midnight 30 September 2020. .

The water of the SFMR clearly warmed as it flowed downstream from the USGS gage to the Phase I restoration site during the periods we examined in mid- to late-summer of both 2019 and 2020. However, the degree of warming varies both across the season and within each day (Figures 21 & 22, Table 6). In general, more warming occurs in midsummer than in late summer or early fall because days are longer and daily solar radiation is considerably greater although these relationships are confounded by changing discharge due to changes in dam operations. At a daily scale, temperature increases are largest for the daily maximum temperature, intermediate for the daily mean temperature, and very small for the daily minimum temperature (Table 6). The comparison between the expected pre-restoration temperature for the Phase 1 reach and the average observed temperature masks potentially interesting responses. In the most extreme case, one temperature data logger recorded a two-week long average of the daily maximum temperature more than 4 °C above the expected temperature. Over the same time period the logger with the coolest daily average temperature recorded an average daily maximum 0.06 °C cooler than the expected pre-restoration temperature (Table 6). Temperature changes of a few 100^{ths} of a degree should be considered as "no change" when considering the overall accuracy of the data loggers. However, the huge range in temperatures measured in just 6 loggers located within the Phase I restored reach is indicative of the high degree of spatial and temporal variability in thermal regimes after restoration.

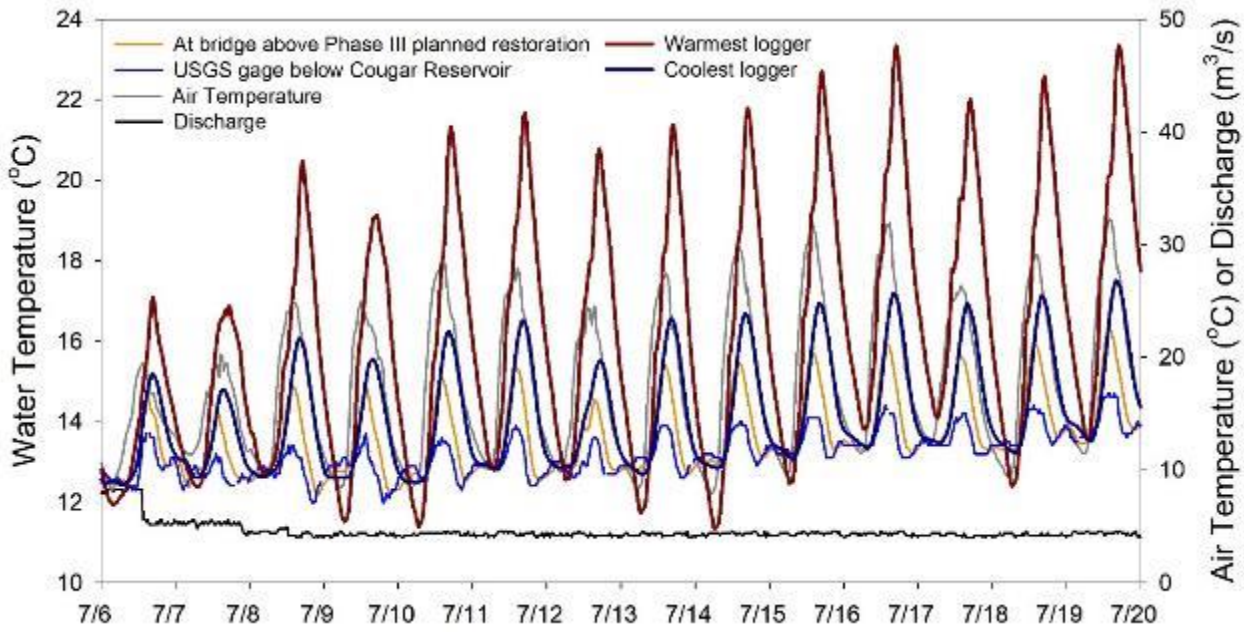

Figure 21: Detailed view of temperature time series, starting from 00:30 6 July 2020 through 23:30 on 19 July 2020. Details are as described in the legend for Figures 19 & 20.

Data collected in 2019, when 34 loggers were deployed in late summer clearly illustrates the spatial heterogeneity in stream thermal regimes. Unfortunately, we did not have a logger located above the restored reach so we cannot estimate the expected pre-restoration temperature within the reach. Still, our data suggest that temporal heterogeneity increased substantially. The standard deviation (SD) calculated for each logger on each day (n=48) and then averaged across all loggers for all days, increased from 0.32 at the USGS gage to 0.76 within the restored reach (Table 7), with the SD for one logger reaching 0.96 – three-times higher than that of water released from Cougar Reservoir. Similarly, the average diel range in water temperatures increased from 1.21 °C to 2.39 °C when averaged across all 34 loggers, with one logger showing close to a 3 °C diel range in temperature when averaged over the entire 42-day monitoring period. Further, the spatial heterogeneity of water temperatures surveyed by thermal infrared was much greater in the restored reach than the mainstem McKenzie River (Figures 23 and 24). While the absolute temperatures of the South Fork and Mainstem McKenzie may be different, we assume that spatial heterogeneity in water temperature, before restoration, would be similar because both the mainstem and the pre-restoration South Fork had simple, single thread channels. However, with only a single point measurement of the mainstem temperature above the restored reach, we have no way of quantifying spatial heterogeneity in water temperature prior to restoration.

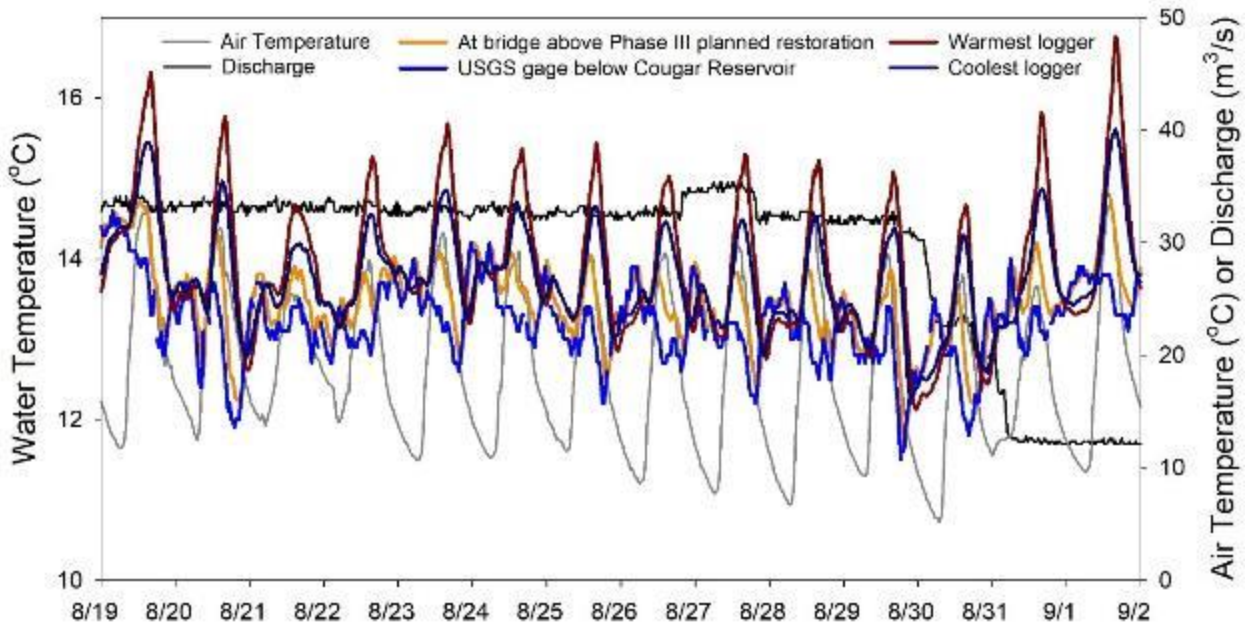

Figure 22: Detailed view of temperature time series, starting from 00:30 19 August 2020 through 23:30 on 1 September 2020. Details are as described in the legend for Figures 19 & 20.

Somewhat surprisingly, our expected pre-restoration average daily minimum temperature in the Phase I reach is cooler than the temperature observed at the FR19 bridge (Tables 6). This is especially surprising because the observed average daily minimum temperatures increase from the USGS gage to the FR19 bridge. However, close inspection of the night-time temperature data in the daily time series (Figures 21 and 22) show that the temperature profile at the USGS gage is complex and on most nights a pulse of warmer water is released from the dam. Also, there appears to be a 1.5 to 2.0 hr lag in the timing of the minimum temperature at the FR19 bridge relative to the USGS gage. We suspect that these time lags, caused by water travel times through the length of the reach, and the complex temperature profile led to errors in our estimate of the expected temperature. Again, these cooling effects are quite small, falling within the accuracy range of the loggers.

The UAS thermal data reported here (Figures 23 and 24) was collected near or soon after the daily maximum temperature on 4 September 2020 (Figure 25), during which time water temperatures at the USGS gage averaged 13.88 °C and ranged from 13.7 °C to 14.0 °C. Based on the rate of heating from the USGS gage to the FR19 bridge, the expected pre-restoration average water temperature would have been 15.82 °C. By comparison, the surface water temperature of the Phase 1 restoration area averaged 20.6 °C and ranged from a minimum of 17.7 to a maximum of 23.8 °C (1st- and 99th-percentiles, respectively). Again, these comparisons should be treated with caution because the accuracy of the thermal infrared imagery has not been validated and because the potential errors in the estimate of the expected pre-restoration temperature are unknown.

Table 6: Comparison of temperatures measured at the USGS stream gage immediately below Cougar Reservoir, at the Forest Road 19 bridge, and the expected temperature at the mid-point of the pre-restoration channel with temperatures observed in HOBO U22 temperature data loggers located in the Phase I restoration reach. The warmest and coolest loggers were selected by their average daily temperatures. The FR19 bridge is located 2.78 km below the USGS gage; the approximate center of the Phase I restoration reach is located 2.86 km below the FR19 bridge. Observations were made from 00:30, 6 July 2020 through 23:30, 19 July 2022.

July 6 through July 19, 2020	Average Daily Maximum Temp. (°C)	Average Daily Temp. (°C)	Average Daily Minimum Temp. (°C)	Diel Range	Daily Standard Deviation
USGS - 14159500	13.91	13.19	12.69	1.22	0.35
Bridge - 10792435	15.29	13.59	12.76	2.53	0.82
Expected Phase I	16.76	14.00	12.60	4.16	1.36
Phase I – Average (n=6)	17.51	14.40	12.61	4.90	1.65
Warmest Logger (10862900)	21.04	16.21	12.48	8.56	2.77
Coolest Logger (10792432)	16.70	14.13	12.77	3.94	1.37
Diff Avg-Expected	0.75	0.40	0.01	0.74	0.29

The surface temperature of the mainstem McKenzie appeared homogenous (Figure 23) with a standard deviation of 0.9 C and a range of 4.2 C, with visibly warmer water being evident along channel edges and a patch west of the Phase 1 outlet. Phase 1 appears more heterogeneous and has a surface temperatures standard deviation of 1.6 C and a range of 6.1 C. with warmer water being present near the edge of accumulated woody material and the stream edge.

The results of the Kamogorov-Smirnov test suggest the surface temperature distributions are significantly different ($p < 0.005$, Figure 24) between the two areas. The two distributions overlap at the upper 10^{th} percentile of the mainstem and lower 10^{th} percentile of the Phase 1 suggesting that the majority of surface temperatures in Phase 1 are simply warmer than the mainstem. The water arriving from upstream of the Phase 1 area also appears warmer than the mainstem as evidenced by the water temperature of the large east to west flowing channel on the eastern edge of the Phase 1 area, suggesting that the water source for the SFMR is warmer than the upstream water sources for the component of mainstem seen here. Based on this thermal imagery and the subsequent statistical analysis it does appear that the restoration treatment accomplished the objective of increasing water temperature heterogeneity in the Phase 1 area, relative to its previous single threaded state. However, additional study and analysis are needed to understand the persistence of this heterogeneity within and between years.

Table 7. Comparison of temperatures measured at the USGS stream gage immediately below Cougar Reservoir and the average, maximum, and minimum values of each metric recorded from 34 temperature loggers in the Phase I restoration reach, located ~5.5 km downstream. Observations were made from midnight 12 August 2019 through midnight 22 September 2019.

August 13 through September 22, 2019	Average Daily Maximum Temp. (°C)	Average Daily Temp. (°C)	Average Daily Minimum Temp. (°C)	Diel Range	Daily Standard Deviation
USGS-14159500	11.05	10.44	9.84	1.21	0.32
Average of 34 Loggers	12.93	11.48	10.55	2.39	0.76
Warmest Logger	13.60	12.09	11.16	2.99	0.96
Coolest Loggers	12.35	11.19	10.37	1.92	0.58
Difference: Average - USGS	1.88	1.04	0.71	1.18	0.44

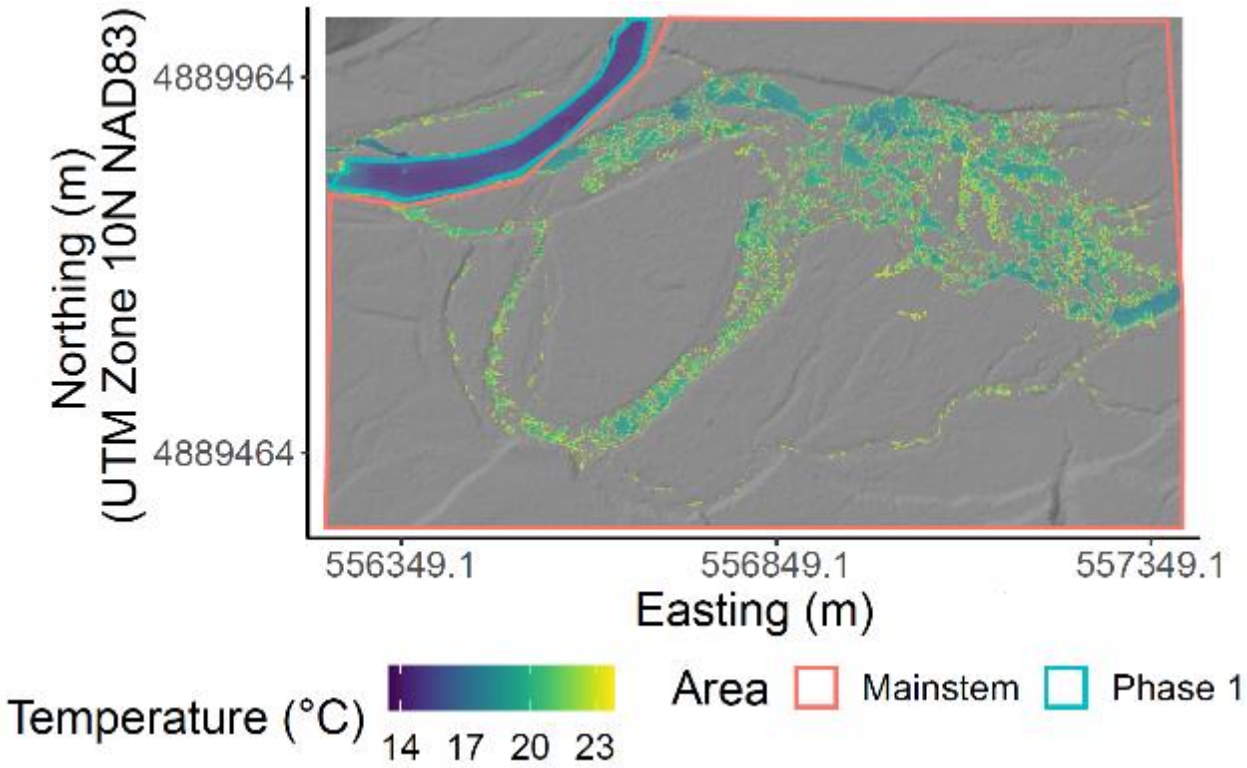

Figure 23: Water temperature derived from UAS imagery of the mainstem McKenzie River and the Phase I restoration reach of the South Fork McKenzie River from 4 September 2020; b) histogram of temperature distribution of mainstem on 4 September

2020; and c) histogram of temperature distribution of Stage-0 restoration reach on 4 September 2020.

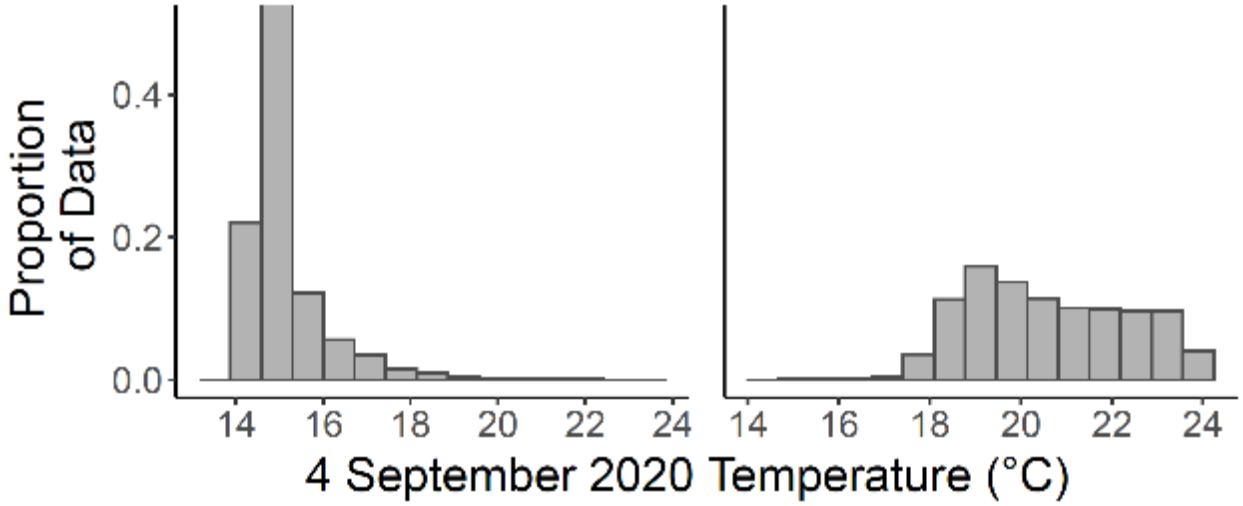

Figure 24: Histogram of water surface temperature distributions of the mainstem McKenzie River and the Phase I restored reach on the South Fork McKenzie River on 4 September 2020.

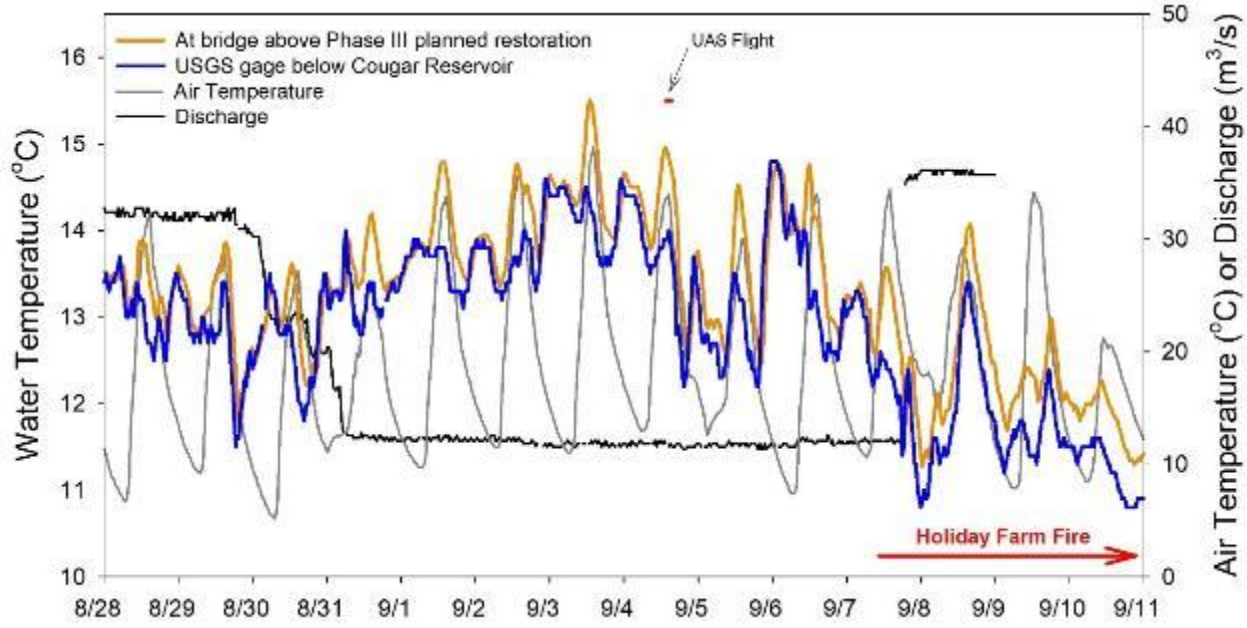

Figure 25: Detailed view of temperature time series, starting from midnight 28 August 2020 through 23:30 on 10 September 2020. Very short red line indicates the time and duration of the UAS flight on 4 September. The bold-red arrow begins on 7 September 2020 with the ignition of the Holiday Farm Fire, which soon thereafter burned over the entire restored reach in a severe, stand-replacing fire.

Discussion – Stream Temperature:

The field temperature monitoring data was collected solely for validation of the thermal infrared imagery collected during the UAS surveys. At OWEB's request, we have moved forward with documenting and archiving our field temperature data with the Oregon Department of Environmental Quality (DEQ). We also conducted a brief preliminary analysis of those data for this final report. We are continuing to pursue additional funding for analysis of the thermal imagery but, as of yet, such funds have not been obtained. In summary – this report details the results of our preliminary analyses; they have not been presented nor published elsewhere.

The restoration of the South Fork McKenzie River, from a simple single thread channel into a widely inundated floodplain appears to contribute to the warming of the river water. This effect is largest when discharge is low in mid-summer when short-wave radiation fluxes are highest. At these times of year, the effect of the restored channel appears to increase mean daily temperatures by 0.4 °C and maximum daily temperatures by 0.75 °C. Data from both the temperature data loggers and the thermal infrared imagery show many areas with unexpectedly high temperatures. The restoration created large areas that were shallowly inundated with low flow velocities. Without shade, water in these locations warms substantially during the day so that by the time of the afternoon UAS flight, the thermal imagery showed that these areas were very warm when compared to the mainstem McKenzie River (Figure 23) or to the temperatures recorded at the USGS gage and projected into expected temperatures within the restored reach. These data support our expectations that the locations with the shallowest water and slowest flow velocities would warm the most during the day whereas locations with deeper water, higher flow velocities, and better longitudinal connectivity through the length of the restored reach would warm the least.

We observed little change in minimum temperatures. Interestingly, the loggers with the highest average daily maximum temperatures also tended to have the lowest average daily minimum temperatures. These results are also consistent with our expectations that shallowly inundated areas with low flow velocities would experience the greatest cooling during the night from energy losses as outgoing long-wave radiation. Such radiational cooling would also occur in locations with deeper water, higher flow velocities, and better longitudinal connectivity through the length of the restored reach, but those radiative losses would have to cool a much larger amount of water so they would have the least effect on water temperature in these locations.

We do not see any evidence in our data to suggest that increased exchange flows between the surface and subsurface environments are cooling water as it flows through the restored reach. The influence of exchange fluxes on stream water temperatures depends on many factors, although both the amount of exchange flow and its residence time in the subsurface will have a large effect (Wondzell, 2011). Exchange flows with subsurface residence times of 10 hours to many days will damp diel variations in temperature because the temperature of upwelling hyporheic water will tend toward the daily mean temperature. Thus, at night, these return flows will tend to be warmer than the stream water but cooler than the stream water during the day (Wondzell, 2012). As a consequence, if hyporheic exchange was large, relative to stream discharge, then we would expect to see smaller diel variations. Instead, we found that diel

variations increased in the restored reach. We have every reason to expect that exchange flows are occurring, and that the amount of exchange flow has increased because the restoration increased the total inundated area. Therefore, the magnitude of the exchange flows must be small relative to total stream discharge and could not mitigate the large and persistent effects of daytime heating from shortwave radiation and nighttime cooling from losses of long-wave radiation. It is likely that the exchange flows would create localized cool-water patches on the streambed and that those patches could be used by aquatic organisms. However, the temperature data loggers were not located within the sediment-water interface and the thermal imagery only measures the water surface temperature. Thus, our monitoring protocols would not be sensitive to fine-scale thermal heterogeneity of cool water patches created by upwelling subsurface water.

The distributed network of temperature data loggers and the thermal imagery both suggest that the restoration slightly warmed the overall water temperature of the South Fork McKenzie River during the summer. These estimates were based on extrapolating the warming that occurred as water flowed through the long, unrestored reach between the USGS gage and the sensor located at the Forest Road 19 bridge and then comparing the expected warming to the observed temperatures in the sensor network. Unfortunately, we are unable to better quantify the exact degree of warming because we lack pre-restoration data. Further, the SFMR now flows into the mainstem at multiple locations across the full width of the restored reach; it does not return to a single thread channel before joining the mainstem. Because we do not know the proportion of the river's discharge that flows through each location where we deployed temperature data loggers, we cannot calculate the net effect of these locations on the river's temperature. Our data definitively show that water warms slightly, by 0.4 °C (average of mean daily temperature) to 0.75 °C (average of maximum daily temperature) with some locations warming by more than 4.0 °C. However, we cannot precisely quantify the net effect of this increase in water temperature as it is delivered to the mainstem McKenzie River.

GENERAL DISCUSSION:

Functionality of UAS-based Monitoring for Stream Restoration:

The overall goal of this project was to explore the use of UAS-based imagery and image analysis to either augment, or perhaps even entirely replace, on the ground field monitoring to track changes over time in streams and floodplains restored to a Stage-0 conditions. We identified 5 critical metrics that appeared conducive to monitoring with UASs: inundated area, large wood, sediment, flow velocity, and water temperature. These physical/geomorphic attributes are often tightly linked to habitat quality. Thus, monitoring changes in these attributes, over time, would provide important information on the effectiveness of the restoration project.

Each of the 5 metrics chosen for the physical/geomorphic monitoring presents substantial challenges to traditional field-based monitoring when extensive areas of the channel and floodplain are restored. Traditional methods are most always transect-based, using cross-sectional transects on single-threaded stream channels. However, restoration to a Stage-0 condition often eliminates any distinct channel and that was certainly the case at the SFMR, where not only was the channel eliminated, but much of the floodplain was also inundated. Further, 1,000s of large logs were placed throughout the restored site, so that field access was difficult at all time and dangerous under high flow conditions. Given the challenges faced by traditional monitoring methods, UAS-based methods offered a potentially safer, less expensive, and more time-efficient alternative while also allowing extensive sampling across the entire restored area and providing a long-term visual record of any changes that might occur over time.

The ability of the UAS-based remote sensing and image analysis to deliver the expected benefits varied greatly by metric. Also, this was expected to change over time as vegetation regrows at the site so that increasingly large areas will be occluded from the UAS survey by the canopies of trees and shrubs, and by herbaceous vegetation.

Inundated Area: The NDVI method used to estimate inundated area was highly effective wherever the water surface was visible to the UAS. The method was quick and easy to employ and gave favorable results. However, the complex spatial patterns of the actual inundated area meant that, in many places along the edge of the inundated area, or where narrow channels or small patches were inundated, the vegetative canopy already limited estimates of inundated area, only a few years after restoration and long-before complete vegetative recover has occurred. We were able to correct for the effects of vegetation, using elevation information from the DEM of the site, but this will become increasingly difficult as the vegetation regrows and also requires a relatively recent DEM.

Large In-Stream Wood: By combining UAS technology, machine learning, and traditional sampling approaches, we demonstrated the potential to estimate large woody debris in a river ecosystem. Importantly, our methods provide accompanying confidence intervals that offer insight regarding the precision of our estimates. Machine learning methods alone lack traditional precision estimates, instead relying on other metrics that are less straightforward to decipher. Additionally, interpretation of aerial imagery acquired via UAS provides an efficient and safer

alternative to approaches that rely on field sampling alone, and UAS are easily deployed compared to piloted aircraft. Potential limitations include estimating wood area in canopy occluded sites. These estimators depend on auxiliary information that can only be obtained where there are unobstructed views of the landscape. Future efforts may incorporate aerial and/or terrestrial LiDAR to acquire data that improve uncertainty in occluded areas. Additionally, basic knowledge of machine learning is a prerequisite to executing the estimator that achieved the highest precision. This requires training data that consist of time-intensive manual image classification for individual flights. However, our imagery is radiometrically calibrated and theoretically should account for differences in incident light between scenes potentially reducing the need to produce multiple sets of training data. Ultimately, managers can utilize these methods to estimate large wood and assess retention through time. This provides critical information regarding salmonid habitat quality and success of restoration efforts.

Flow Velocity: Using LSPIV software (e.g. PIV and RIVeR) to analyze high resolution videos (4k video resolution; ~1 cm GSD) for velocity-related metrics revealed promising results. Due to poor georeferencing accuracy and lack of monuments in the field, the sample size of paired field and UAS plots were relatively sparse over space and time. However, the distribution of field based velocities from a flowmeter showed overlap with the distributions of LSPIV velocity estimates. The added benefit is the LSPIV method produces other metrics that are potentially useful to understanding physical process on the site, such as vorticity and flow direction. Additional study is necessary to understand how useful these data are to informing habitat suitability, bioenergetics, and hydrological models. Furthermore, additional study is necessary to fully understand the efficiency of this method relative to conventional field measurements. It took nearly 4 flight hours with a Phantom IV to collect 40 video plots randomly distributed across the entire Phase 1 area. Processing of the 27 video plots presented here took over 50 hours of computer time and about 35 hours of technician time. Since much of the technician time was learning the software, developing the workflow, and troubleshooting, there is likely room to improve efficiency using the software. Overall the results suggest the method has merit, but requires additional refinement and study to fully characterize efficiency and tradeoffs of the method.

Sediment: The use of high-resolution imagery (sub-cm) in conjunction with BASEGRAIN software to derive sediment size distributions using image granulometry was not as effective as desired. Processing of the small number of plots took over 50 hours of technician time. Converting that time to in-field gravelometer measurements would have yielded many more observations to facilitate inference on sediment size distribution. It is important to note that much of the 50 hours was spent learning the software and troubleshooting issues with the imagery. In a professional production workflow, this could likely be optimized, substantially reducing time per plot. As it stands, we do not recommend operationalizing the method as implemented here. In the sediment analysis section we present several suggestions for improving the method and cite recent literature that shows promising results with BASEGRAIN and alternative methods for image-based granulometry. While it would likely take significant effort to develop the image granulometry method for operational implementation at SFMR, we are of the opinion following the 2021 field season that the treacherous and increasingly dangerous field conditions warrant further development if understanding spatio-temporal variation and change of sediment continues to be a subject of interest to management in the future.

Costs and Special Requirements of UAS-based Monitoring:

In the section below, Budget Accounting, we detail the direct and *in-kind* costs of this project to definitively illustrate the potential expenses of using UAS remote sensing platforms for monitoring. Note that it is difficult to track the exact amounts because resources were shared among sub-groups working together on the larger project and we did not have a definitive way of tracking actual *in-kind* expenses. Despite these limitations, the estimated direct costs are reasonably accurate; the *in-kind* expenses are less so. The UAS-based monitoring approaches initially appear to be convenient because they are potentially quick and relatively inexpensive. And in fact, a complete site survey with the UAS, making both an extensive survey of the entire restored site and collecting relatively "close-up" video imagery of ~40 field plots took only six flight hours (over two days) with a cost ~$4,000, which includes the production of orthomosaics and digital surface models, but not the follow-on processing and analysis to address the five specific factors we targeted here. Note, this cost does include the cost to install the ground-control points that are necessary to precisely georeference and scale the orthomosaics and surface models. Of the $4,000 cost, about $1000 is post-processing, $1000 is the full area survey and $2,000 is associated with collecting the 40 video plots, which puts cost to about $50/plot or $0.97 / m^2. Since the remaining $2000 is the full area survey, that breaks down to about $33 / hectare or $0.0033 / m^2. For the sediment and velocimetry, these plots turned into 1000+ data points for each plot where such analyses were appropriate. For temperature, this produced about 150,000 stream surface temperature estimates, and for large wood, these data produced about 2.7 million data points used to inform the GREG estimator analysis

The actual cost of field work was difficult to disentangle from the total because it was partially covered through cost sharing agreements, so we make some assumptions and use Oregon State University's vehicle cost estimates ($25/day + $0.31 / mile) and average graduate student rates ($26 / hr + 38% other payroll expenses) for the sake of facilitating a cost comparison to UAS data collection. For 2019's field campaign, it took two people working approximately twelve, ten hour days or 200 hours to install and measure the 36 plots. In addition to about 50 hours in total for site orientation and field protocol development, testing, and training. For 2020, time was reduced to about 100 hours in the field, with some efficiency gained from using the same personnel from the previous season and reducing sampled plots to 23. In 2021, this was further reduced to about 72 hours in the field to re-measure just 15 field plots. Since the plot data was captured with ArcGIS Survey123, the data was nearly analysis-ready after field collection, and only takes about took hours of processing for each of the field campaign years. Graduate students were used for this work, and Oregon State University states that the average hourly rate is $26/hr with other payroll expenses of 38% (as of 2022) which brings the total to approximately $36 / hr. Multiplied $36 / hr by 378 hours (100+72+200+6) = $13,608 plus the cost of transport to/from site. Transport and lodging costs were highly variable, so for the sake of comparison, assume the field crew camped on site. Vehicle rentals at Oregon State University currently cost $25 / day; and field work took 12, 5, and 3 days for 2019, 2020, and 2021, respectively, resulting in $500 plus mileage expenses which we assumed were about 400 mi/year * $0.31 /mile = $372. Given the coarse assumptions, it's reasonable that total cost for field work was about $15,000 or $129 per plot. Although each plot represents about 52 m^2 on the ground, only about 12.5 m^2 are actively surveyed, which breaks this down to about $10 / m^2.

For sediment this amounts to a maximum of 40 sediment samples per plot, 4 velocity observations per plot, 12.5 m^2 of wood area estimates per plot, and one temperature estimate (2021 only; does not include the instream temperature data loggers installed on some plots in 2019). Note that inundated area analysis was not possible from field plots as installed, but would likely be possible with the addition of a total station or auto level survey that was not part of this study. Relative to the UAS survey, cost per m^2 was about 10x at the plot level, additionally, data densities were multiples orders of magnitude lower.

This apparent low cost, high data density, and ready convenience of the UAS remote sensing approach is deceptive, however. The imagery itself is only useful after substantial post-processing, making it ready for various analyses. Both the post-processing and the subsequent analyses require highly skilled personnel with ready access to a variety of software platforms, some of which are proprietary and expensive to license. For example, the PIV software for the velocimetry analysis requires a Matlab license and above-median computer (at least 32 GB of RAM, solid state hard drive, and modern i7 multi-core CPU). It is unlikely that either local Ranger District offices or Watershed Councils will already have staff with these specialized skills, licensed software, or equipment. Not to mention the fact that UAS piloting is technical on its own, and the combined cost of the UAS equipment demonstrated here was nearly $20,000. Therefore, they too would have to contract out these additional analyses at a cost some 5x to 10x the cost of the initial UAS surveys. These "hidden costs" may make UAS-based monitoring prohibitive until such time that local IT and geospatial staff commonly have necessary training and experience using these specialized analytical methods or until the methods are developed to such an extent that they become readily accessible to IT and geospatial staff with more traditional skill levels. Note that for projects involving the USFS, the USFS Geospatial Technology and Application Center has access to personnel who have much of the requisite expertise, and there are support vehicles available to National Forests to utilize these services

Efficiency and Efficacy

Efficiency is interpreted and evaluated many ways with the goal of identifying an optimal course of action given specific criteria. Burches and Burches (2020) describe efficiency in management settings as doing something in the most economical way, and efficacy as producing the desired effect. The intent of this research was to follow the approach of Lister *et al.* (2020) to contrast statistical and economic efficiency between field and UAS approaches. However, for numerous technical, logistical, financial, and personnel reasons described throughout this report, such a comprehensive analysis was not possible. As such, we simply present the fact that cost per collected data point were orders of magnitude lower using UAS and point out that when the hidden costs of processing and analysis are factored in and the practical barriers to implementation are considered, the economic advantage becomes less obvious. However, from the standpoint of efficacy, there appears to be merit in all the UAS remote sensing presented here. We demonstrate that it is feasible to use UAS to safely evaluate inundated area, wood, velocity, and surface temperature broadly across space and time, on a relatively open site like Phase 1 of SFMR, although additional data collection and analysis is necessary to fully characterize the differences between field and UAS estimates. That said, we recommend additional research rigorously examining the economical and statistical efficiencies between the two approaches before a conclusive statement on efficiency can be made. Finally, for those who

may find the results presented here discouraging or ambiguous, we want to mention that UAS technology and processing software is ever evolving, and as automated processing routines come available, and RTK drones become more ubiquitous, processes like those presented here will inherently become more refined and economic advantage will likely become more obvious.

Using and Interpreting the UAS data

The UAS data as presented here were not examined consistently enough to evaluate all 5 factors in the context of pre and post restoration as well as post restoration change 2019 – 2021. This limitation was imposed primarily because each of the five components are at different stages of development (for example large wood analysis was started from scratch), and because the primary focus of the work as presented here was to facilitate comparison to field and UAS methods.

The large wood method as presented allows a global summary of total wood area that can be applied yearly to the low-flow 2019 – and 2021 data to examine global change trends and facilitate intra-site spatial trends as well. This information might be useful for spatially explicit habitat suitability modeling and bioenergetics models that incorporate large wood.

The inundated area method as presented here facilitated a comparison of pre and post treatment condition and quantified the obvious change in area. Such an analysis can also be conducted across time, to examine how inundated areas are changing yearly and allow managers to consider how that corresponds with spawning habitat.

Similarly, to inundated area, the UAS thermal analysis presented here facilitated a comparison to a surrogate of pre-treatment condition relative to post treatment condition. Post-treatment exhibited significantly more thermal heterogeneity, which was the intent of the restoration treatment.

The velocity analysis facilitated an examination of velocity at multiple plots, and while what is presented here was limited to a small number of plots where alignment with field data was acceptable, there are almost 40 plots per year that when processed, analyzed, and summarized, would provide a broader assessment of general velocity trends, and velocity vector trends. Not examined, but of potential use are the vorticity data that may provide insights on fish habitat quality, as well as the intra-plot variability of velocity, which may be useful for considering how stream morphology may be changing across time and at different dam discharge levels.

The sediment analysis as presented is not useful for management purposes because the low sample size of processable plots and the disagreement between field and UAS data call into question the utility of the data. However, sediment was one of the most time-consuming aspects of the field assessment and the field data exhibited extreme variation suggesting that more plots would be necessary to better characterize the sediment size distribution. As such we recommend implementing the recommended changes to the method and drawing inspiration from other successful implementations to more efficiently evaluate sediment with UAS.

Overall, the UAS method presented here has the potential to characterize site conditions for four of the five factors considered. At a minimum these data provide a reference condition for which to compare subsequent surveys (perhaps in 10 year resampling intervals). For management purposes, the large wood and inundated area offer seem to be more readily integrated into existing decision making models and analytical approaches. However, the velocity and thermal data presented here exist at a higher spatial extent and data density than existing habitat suitability models are prepared to ingest and thus must be simplified to plot level averages, vastly under utilizing the data available, further reducing the value added of UAS.

Changes from Original Project Design:

Overall, the physical/geomorphic monitoring sub-project followed the original project design with surprisingly small deviations, given that the stand-replacing Holiday Farm Fire and a global pandemic occurred during the project.

We did have problems acquiring UAS imagery at high flows during the spring leaf-off period. First, flows are controlled by US Army Corps of Engineers (US-ACE) operations of Cougar Dam. A number of external factors has drastically limited the flexibility of the US-ACE to provide high flows during weather windows in the late winter or early spring that are suitable for UAS surveys. Thus spring, high-flow UAS surveys were only completed in 2019 and 2020, but not in 2021 or 2022.

We were unable to sample as many field-validation plots as we had originally planned. We selected a total of 40 plots to be measured in 2019, but our field methods and plot access made work slower than expected so that we only measured 36 plots. We planned to remeasure all of these plots in 2020, but, because of the pandemic, we came close to canceling our field season. However, we had an unexpected opportunity to mount a short field campaign in the late summer to remeasure the field validation plots in the weeks before the UAS survey. Both the number of people and time available were limited, so the field crew was only able to remeasure 23 field plots in 2020.

The Holiday Farm Fire was an unexpected complication for our project. Fortunately, we had just completed the UAS survey and field-plot remeasurements in the weeks before the fire. We were able to get permission from the USFS to access the site soon after the fire and conducted a second post-fire wide-area UAS survey of the entire Phase I restoration site. The pre-fire survey was conducted on 9/4/2020. The "*extra*" post-fire survey was conducted on 11/4/2020.

Plans for Continued Monitoring:

Plans for continued monitoring are uncertain. The original project design planned for Phase III restoration to be completed in 2021 (see Table 1) and post restoration monitoring, funded by OWEB during Oregon's 2021-23 funding biennium, to be completed by summer 2023. Because of the Holiday Farm Fire, these plans have changed. The Phase III restoration has been expanded to include a large area previously occupied by the USFS's Delta Campground located on the peninsula between the SFMR and mainstem McKenzie Rivers (Figure 26). The expanded Phase

III restoration has been subdivided into 3 primary activities (boundaries not shown in Figure 26). Phase IIIa - the decommissioning of Delta Campground – is scheduled for Fall 2022 or summer 2023. Restoration activities in 2023 will focus on Quartz Creek and the Finn Rock Reach so that Phase IIIb – floodplain and back-channel restoration activities not directly tied to SFMR wetted channel – is scheduled for 2024. Currently, Phase IIIc – restoration of the channel and channel adjacent areas covering most of the "original" Phase III area – is scheduled for 2025.

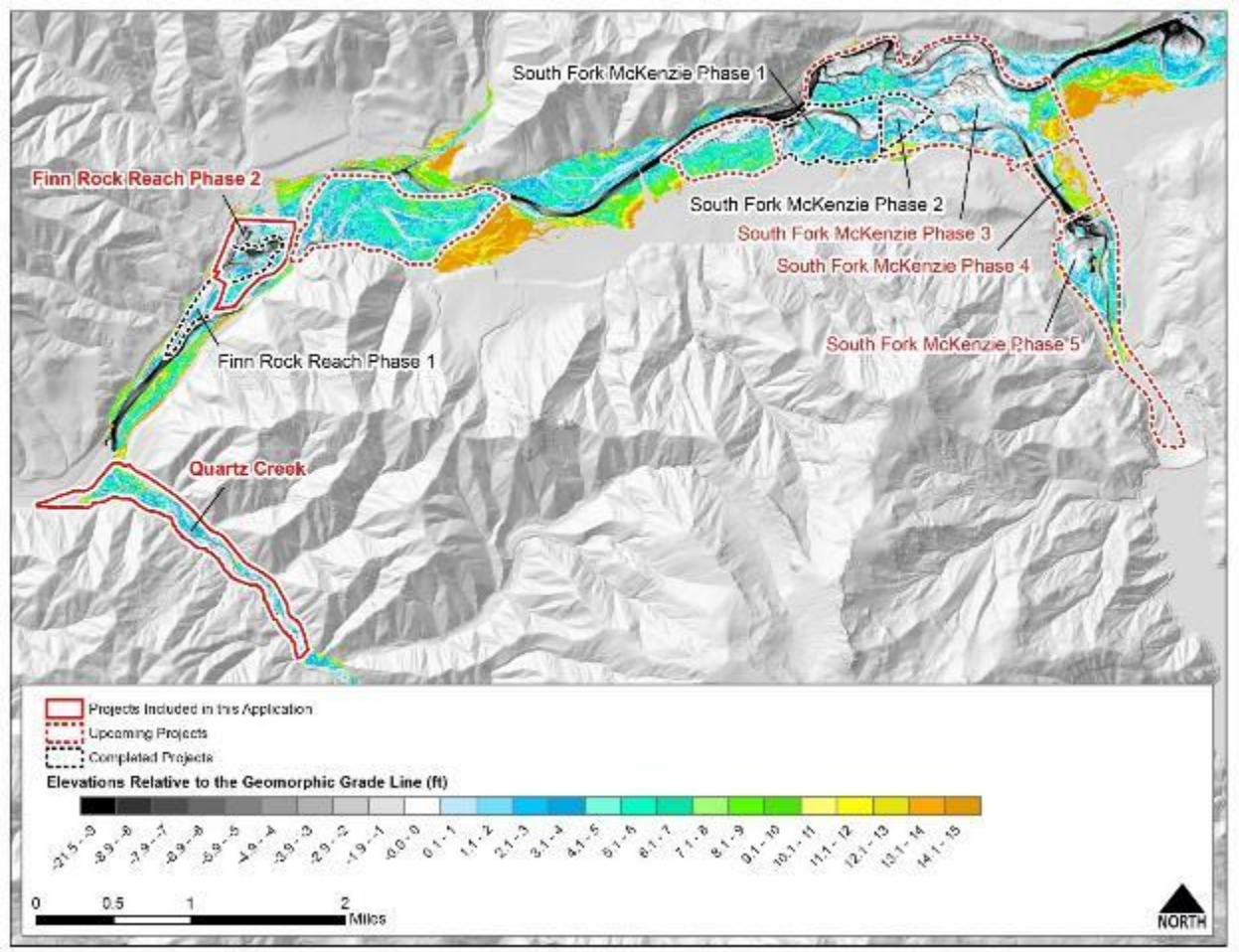

Figure 26: Map of an approximately 6-mile-long section of the mainstem McKenzie River near the town of Blue River, OR., showing the locations of river and valley-floor restoration activities in Quartz Creek (lower-left), South Fork McKenzie River below Cougar Dam (right side) and the mainstem McKenzie River. Color fills show surface elevations relative to a geomorphic grade line (see Powers et al., 2019 for a description of the geomorphic grade line approach).

We "paused" monitoring work at the SFMR because of these delays. We are completing the monitoring, analyses, and evaluation started with OWEB's 2019-2021 biennium funding (described in this report). We are also re-assessing plans for future monitoring. Personnel changes from moves (geographic relocation), promotions, and retirements make for uncertain projections so far into the future. These personnel changes mean that the PNW Research Station

currently has much reduced capacity to continue the detailed UAS monitoring and image analysis planned in the original proposal. Because of these changes, the PNW Research Station contracted out much of the image analysis at considerable direct expense (see the section on Budget Accounting). And while the PNW Research Station was committed to completing the work described in the original proposal, it cannot extend that commitment so far into the future (e.g., Oregon's 2025-2027 budget biennium).

Lessons Learned and Recommendations:

This SFMR monitoring project would have been much more effective had plans for monitoring been developed hand-in-hand with plans for the restoration treatments. Ideally, such planning would have begun several years prior to implementing the restoration, giving time to develop monitoring protocols and identify and install monitoring sites at least one full year before starting the on-ground restoration work. All aspects of the project would have benefited from developing the monitoring plan in concert with the restoration plan. As a specific example, efforts to interpret the temperature monitoring data were continually hampered by the lack of pre-restoration data. Two reference loggers, one located immediately above, and a second located immediately below the restored reach and installed at least one full year before the restoration and kept in exactly the same place throughout the entire post-restoration monitoring period would have provided the information necessary for estimating temperature changes resulting from the restoration. A more spatially extensive network of pre-restoration data loggers would have been necessary to evaluate changes in the spatial heterogeneity of the site's thermal regime. Similarly, this network would need to be installed at least one full year before the restoration and reinstalled in the same locations (to the degree possible) after the restoration.

Overall, the project would have benefitted from better communication between the research scientists and the restoration practitioners. Such communication is understandably difficult. Each group faces different pressures, has different timelines and goals, and measures accomplishments in different ways. A better understanding and explicit acknowledgement of these differences at the outset might have helped. Close coordination between scientists and managers is also vital as each group had different responsibilities for the overall monitoring, and often, data from one subproject was needed to provide context for analysis and interpretation of data collected in another subproject. Thus, sampling needs to be coordinated and methods need to be applied with exacting consistency over time. This was not always achieved as external pressures or frustrations caused by the difficulty of continuing to apply the original monitoring methods in the post-restored conditions led to changes. Unfortunately, changing methods in the middle of long-term monitoring projects makes it difficult to identify the cause of any change that is observed: Were the changes real? Or were they simply artifacts of the change in the methods used? Maintaining close working coordination requires a substantial time commitment but finding that time can be challenging when all involved are facing pressures to get work done while understaffed and facing tight deadlines. This is a problem for both scientists and managers. As is the lack of flexibility to be able to adjust sampling methods to better meet immediate complexities and changing realities. However, these investments of time for communication and commitments to maintain consistent methods are necessary for success of restoration and monitoring projects.

I am unsure how we could have improved communication. Certainly, this was a shared responsibility among both researchers and managers, and both groups started the project with excitement, enthusiasm, and intentions to work together. However, external forces tended to push each subgroup to work with a degree of independence and isolation, which was then further exacerbated by the pandemic. I do think that regular project meetings, at monthly or two-month intervals, that included updates and report-outs from each group and sub-group would have helped. As would holding such meetings in person and in a way that allowed for casual or un-scheduled interactions among people working on the project. However, it is often difficult to hold meetings with even a moderately large group when each person has a busy and full calendar. Further, as a project co-lead lacking administrative help, organizing such meetings is time consuming. Still, this sort of formal and informal communication during face-to-face meetings can be critically important to project success.

GENERAL CONCLUSIONS:

The overall goal of this project was to explore the use of UAS-based imagery and image analysis to either augment, or perhaps even entirely replace, ground-based field monitoring to track changes over time in streams and floodplains restored to a Stage-0 conditions. We identified 5 critical metrics that appeared conducive to monitoring with UASs: inundated area, large wood, sediment, flow velocity, and water temperature. Each of these metrics presented substantial challenges to traditional field-based monitoring when extensive areas of the channel and floodplain were restored. Given the challenges faced by traditional monitoring methods, UAS-based methods offered a potentially safer, less expensive, and more time-efficient alternative while also allowing extensive sampling across the entire restored area and providing a long-term visual record of any changes that might occur over time. Our results showed that the ability of the UAS-based remote sensing and image analysis to deliver the expected benefits varied greatly by metric. For example, inundated area was relatively easy to extract from the imagery whereas substantial challenges in segmenting individual sediment clasts suggests that monitoring of sediment size class distributions is currently beyond the capacity of the techniques readily available today. Automated processes reliably identified the surface area of large pieces of instream wood, and both velocimetry and the UAS thermal imagery appeared to offer interesting opportunities to provide relatively fine-grained information over relatively large spatial extents but needed more development to realize these opportunities. Clearly, not all aspects of the UAS-based remote sensing are equally mature, but overall, we found that the UAS-based remote sensing and image analysis seemed to provide a promising alternative to monitoring for some metrics.

We also want to add two cautionary notes: First, we remain concerned that regrowth of vegetation will create problems for long-term monitoring schemes. Remote-sensing techniques require that things of interest be visible in the imagery. However, as vegetation regrows at the site, we expect that increasingly large areas will be occluded from the UAS survey by the canopies of trees and shrubs, and by herbaceous vegetation. This change in the area of the restored reach amenable to UAS surveys may bias efforts to monitor long-term trends. Second, while UAS-based monitoring approaches may appear to be convenient because they are potentially quick and relatively inexpensive, this apparent low cost and ready convenience may be deceptive. The UAS imagery requires substantial post-processing to make it ready for various analyses. Both the post-processing and the subsequent analyses require highly skilled personnel with ready access to a variety of software platforms, some of which are proprietary and expensive to license. It is unlikely that either local Ranger District offices or Watershed Councils will already have staff with these specialized skills and licensed software. Therefore, they too would have to contract out these additional analyses at a cost some 5x to 10x the cost of the initial UAS surveys. These “hidden costs” may make UAS-based monitoring prohibitive until such time that local IT and geospatial staff commonly have necessary training and experience using these specialized analytical methods or until the methods are developed to such an extent that they become readily accessible to IT and geospatial staff with more traditional skill levels.

REFERENCES:

Baron, J. S., N. L. Poff, P. L. Angermeier, C. N. Dahm, P. H. Gleick, N. G. Hairston Jr., R. B. Jackson, C. A. Johnston, B. D. Richter, and A.D. Steinman. 2002. Meeting ecological and societal needs for freshwater. Ecological Applications, 12(5), 1247–1260.

Bechtold, W.A. & Patterson, P.L. (2005) The enhanced forest inventory and analysis program-national sampling design and estimation procedures. Gen. Tech. Rep. SRS-80. Asheville, NC: US Department of Agriculture, Forest Service, Southern Research Station. 85 p., 80.

Burches, E., & Burches, M. (2020). Efficacy, effectiveness and efficiency in the health care: the need for an agreement to clarify its meaning. Int. Arch. Public Health Community Med, 4, 35.Buscombe, D. 2020. SediNet: A configurable deep learning model for mixed qualitative and quantitative optical granulometry. Earth Surface Processes and Landforms, 45(3), 638-651.

Buscombe, D. 2020. SediNet: A configurable deep learning model for mixed qualitative and quantitative optical granulometry. Earth Surface Processes and Landforms, 45(3), 638-651.

Buscombe, D. 2013. Transferable wavelet method for grain-size distribution from images of sediment surfaces and thin sections, and other natural granular patterns. Sedimentology, 60(7), 1709-1732.

Chen, X., Hassan, M. A., & Fu, X. 2022. Convolutional neural networks for image-based sediment detection applied to a large terrestrial and airborne dataset. Earth Surface Dynamics, 10(2), 349-366.

Cluer, B. and C. Thorne. 2014. A Stream Evolution Model Integrating Habitat and Ecosystem Benefits. River Research and Applications 30, 135–154. doi:10.1002/rra.2631

Engle, F. 2020. Video Stabilizer. GitHub Repository. United States Geological Survey. Last accessed on 8/12/2022 at https://github.com/frank-engel-usgs/Video-Stabilizer.

Farid, H., & Woodward, J. B. (2007). Video stabilization and enhancement. TR 2007-605, Dartmouth College, Computer Science.

Godfrey, J., Roshwalb, A., and Wright, R.L. 1984. Model-Based Stratification in Inventory Cost Estimation. Journal of business & economic statistics 2(1): 01-09. doi:10.1080/07350015.1984.10509365.

Dawson, S. M., M. H. Bowman, E. Leunissen, S. Pascal. 2017. Inexpensive Aerial Photogrammetry for Studies of Whales and Large Marine Animals. Frontiers in Marine Science 4, DOI=10.3389/fmars.2017.00366 https://www.frontiersin.org/articles/10.3389/fmars.2017.00366

Detert, M., and V. Weitbrecht. 2013. User guide to gravelometric image analysis by BASEGRAIN. pgs. 1789-1795, *in*: S. Fukuoka, H. Nakagawa, T. Sumi, H. Zhang (eds.). Advances in River Sediment Research. CRC Press, London, UK. 165 p. https://doi.org/10.1201/b15374.

Detert, M., and V. Weitbrecht. 2020. Determining image-based grain size distribution with suboptimal conditioned photos. pgs. 1045-1052, In: Uijttewaal, W., Franca, M. J., Valero, D., Chavarrias, V., Arbós, C. Y., Schielen, R., and Crosato, A., (eds.). River Flow. CRC Press, London, UK. https://doi.org/10.1201/b22619, 2020.

Lang, N., Irniger, A., Rozniak, A., Hunziker, R., Wegner, J. D., & Schindler, K. 2021. GRAINet: mapping grain size distributions in river beds from UAV images with convolutional neural networks. Hydrology and Earth System Sciences, 25(5), 2567-2597.

Lewis, Q. W., Lindroth, E. M., & Rhoads, B. L. 2018. Integrating unmanned aerial systems and LSPIV for rapid, cost-effective stream gauging. Journal of Hydrology, 560, 230-246.

Lister, Andrew J.; Andersen, Hans; Frescino, Tracey; Gatziolis, Demetrios; Healey, Sean; Heath, Linda S.; Liknes, Greg C.; McRoberts, Ronald; Moisen, Gretchen G.; Nelson, Mark; Riemann, Rachel; Schleeweis, Karen; Schroeder, Todd A.; Westfall, James; Wilson, B. Tyler. 2020. Use of Remote Sensing Data to Improve the Efficiency of National Forest Inventories: A Case Study from the United States National Forest Inventory. Forests. 11(12): 1364. 41 p. https://doi.org/10.3390/f11121364.

MathWorks. 2014. MATLAB Release 2014b, The MathWorks Inc., Natick, MA.

McConville, K.S., Moisen, G.G., and Frescino, T.S. 2020. A Tutorial on Model-Assisted Estimation with Application to Forest Inventory. Forests 11(2): 244. doi:10.3390/f11020244.

Nobre A. D., L. A. Cuartas, M. Hodnett, C. D. Rennó, G. Rodrigues, A. Silveir, M. Waterloo, S. Saleska. 2011. Height Above the Nearest Drainage – a hydrologically relevant new terrain model. Journal of Hydrology 404 (1-2) 13-29.

Patalano, A., García, C. M., & Rodríguez, A. (2017). Rectification of Image Velocity Results (RIVeR): A simple and user-friendly toolbox for large scale water surface Particle Image Velocimetry (PIV) and Particle Tracking Velocimetry (PTV). Computers & Geosciences, 109, 323-330.

Powers, P. D., M. Helstab, and S. L. Niezgoda. 2019. A Process-based Approach to Restoring Depositional River Valleys to Stage 0, An Anastomosing Channel Network. River Research and Applications 35(1), 3–13.

Rains, A. 2019. A comparative Analysis of Grain Size distributions and Cross Sections using an Oblique Photoset on the Nisqually Riverbed Adjacent to Longmire In Mount Rainier National Park. University of Washington Masters Thesis. Last accessed 1 August 2022 https://digital.lib.washington.edu/researchworks/handle/1773/45019.

Rosenfeld, J. S., Campbell, K., Leung, E. S., Bernhardt, J., & Post, J. 2011. Habitat effects on depth and velocity frequency distributions: Implications for modeling hydraulic variation and fish habitat suitability in streams. Geomorphology, 130(3-4), 127-135.

Sass, G.G. 2009. Coarse Woody Debris in Lakes and Streams. In Encyclopedia of Inland Waters. pp. 60-69.

Sutarto, T. E. 2015. Application of large-scale particle image velocimetry (LSPIV) to identify flow pattern in a channel. Procedia Engineering, 125, 213-219.

Tauro, F., Petroselli, A., & Arcangeletti, E. 2016. Assessment of drone-based surface flow observations. Hydrological Processes, 30(7), 1114-1130.

Thielicke, W., and R. Sonntag. 2021. Particle Image Velocimetry for MATLAB: Accuracy and Enhanced Algorithms in PIVlab. Journal of Open Research Software, vol. 9, doi:10.5334/jors.334.

Thompson, S.K. 2012. Sampling. 3rd ed. ed. Wiley series in probability and statistics. Wiley, Hoboken, N.J.

Wondzell, S. M. 2011. The role of the hyporheic zone across stream networks. Hydrological Processes 25: 3525-3532.

Wondzell, S. M. 2012. Hyporheic Zones in Mountain Streams: Physical Processes and Ecosystem Functions. Stream Notes January-April 2012, Stream System Technology Center, Rocky Mountain Research Station, Ft. Collins, CO.

Woodall, C. and Williams, M.S. 2005. Sampling protocol, estimation, and analysis procedures for the down woody materials indicator of the FIA program.

SUMMARY OF PRODUCTS:

Publications to Date:

Flitcroft, R., W. R. Brignon, B. Staab, R. Bellmore, J. Burnett, P. Burns, B. Cluer, G. Giannico, M. Helstab, J. Jennings, C. Mayes, C. Mazzacano, L. Mork, K. Meyer, J. Munyon, B. Penaluna, P. Powers, D. N. Scott, and S. Wondzell. (*revised and resubmitted*). Rehabilitating Valley Floors to a Stage-0 Condition: A Synthesis of Opening Outcomes. Submitted to Frontiers in Environmental Science.

Hinshaw, S.K. 2022. Monitoring spatial heterogeneity and carbon sequestration in restored river-wetland corridors. PhD Dissertation. Colorado State University, Fort Collins, CO.

Hinshaw, S., E. Wohl, J. D. Burnett, S. Wondzell. 2022. Development of a geomorphic monitoring strategy for Stage-0 restoration in the South Fork McKenzie River, Oregon, USA. Earth Surface Processes and Landforms DOI: 10.1002/esp.5356

Presentations to Date:

Primary Presentations:

Barker, M.I., Burnett, J.D., Gutierrez, F., and Wing, M. G. 2021. Estimating Two-Dimensional Wood Area from UAS Imagery. Pacific Northwest Aquatic Monitoring Partnership Remote Sensing Forum, 5 October 2021.

Barker, M. I., Burnett, J.D., and Wing M.G. 2019. Automatic Methods for Detecting and Quantifying Large Wood Using UAS Imagery. Oregon Conservation Partnership: Drones and Low-Elevation Imagery, 19 September 2019.

Barker, M.I., Burnett, J.D., and Wing, M.G. 2020. Automatic Methods for Quantifying Coarse Woody Debris from Unmanned Aircraft Systems Imagery. Western Forestry Graduate Research Symposium, Virtual Symposium, 30 April 2020.

Bellmore, R., B. Flitcroft, S. Wondzell, and B. Penaluna. 2019. Evaluating Physical and Ecological Responses to Stage-0 Restoration. Joint presentation at the USFS Region 6 Fish and Watershed Program Managers Meeting. 23-25 April, 2019. Seaside, OR.

Hinshaw, S.K. 2020. Geomorphic field plots for monitoring Stage-0 restoration. Virtual training for Deschutes Land Trust, available on YouTube (https://youtu.be/aTFfsHEhTyw). 18 June 2020.

Hinshaw, S.K., Burnett, J., Nicolato, K., Wondzell, S., and Barker, M. 2019. Monitoring strategy for Stage-0 restoration in the South Fork McKenzie River, Oregon. Binghamton Geomorphology Symposium poster presentation, Denver, CO. Poster PDF available upon request. 12 October 2019.

Hinshaw, S.K. and Scamardo, J.E. 2020. Finding the right fit: post-project monitoring options at reach to valley scales part II- Geomorphic monitoring of a total valley reset: South Fork McKenzie River, Oregon. Riverscape Restoration Network virtual meeting, 12 November 2020.

Wondzell, S. M. and 28 co-authors. 2020. Restoration Overview: South Fork McKenzie River. Oregon Watershed Enhancement Board, Stage-0 Monitoring and Restoration Workshop, Virtual Meeting, 5-6 November 2020.

Related Presentations:

The following presentations were partially based on, or included information collected through this OWEB-funded monitoring program.

Hinshaw, S.K. 2021. Monitoring strategies and carbon storage potential in process-based stream restoration. GeoSlam Lightning Talk virtual presentation for Colorado State University Department of Geosciences Geotechnical Advisory Committee. 1 April 2021.

Hinshaw, S.K. 2021. Why is stream heterogeneity important, and how do we achieve it? Course lecture for Botany/Zoology/Fish and Wildlife 568: Sustaining River Ecosystems in a Changing World (undergraduate/graduate level). Colorado State University, Fort Collins, CO, 24 February 2021.

Hinshaw, S.K. 2022. Monitoring spatial heterogeneity and carbon sequestration in restored river-wetland corridors. PhD Dissertation Defense, Fort Collins, CO, 12 May 2022.

Hinshaw, S.K. and Scamardo, J.E. 2021. Examples and applications of floodplain restoration part II: Stage-0 restoration. Sustaining Colorado Watersheds annual conference, Avon, CO 10 October 2021.

Hinshaw, S.K. and Wohl, E.E. 2021. Quantitatively estimating carbon sequestration potential in soil and large wood in the context of river restoration. American Geophysical Union Fall Meeting, New Orleans, LA, available on YouTube (https://youtu.be/Bk4RXKIutFI). 14 December 2021.

Hinshaw, S.K., and Wohl, E.E. 2022. Quantitatively estimating carbon sequestration potential in soil and large wood in the context of river restoration. Society of Wetland Scientists: Rock Mountain Chapter Annual Meeting, Denver, CO, 6 April 2022.

Hinshaw, S.K., and Wohl, E.E. 2022. Quantitatively estimating carbon sequestration potential in soil and large wood in the context of river restoration. Brown Bag Lunch Talk for Headwaters Corporation, Fort Collins, CO and virtual, 5 April 2022.

BUDGET ACCOUNTING:

The SFMR Stage-0 monitoring project received a total of $201,300 in direct funding from the Oregon Watershed Enhancement Board. Of the direct funding from OWEB, only $16,000 was budgeted for the physical/geomorphic monitoring described in this sub-report. We also estimated that partners' direct contributions and *in-kind* expenses would total $411,594 for the entire project, of which $90,500 would be contributed by the PNW Research Station towards the physical/geomorphic monitoring. Towards the end of the project, the grant administrator allocated an additional $4,000 to extend the physical/geomorphic monitoring through the summer of 2022, so that **direct funding from OWEB totaled $20,000**.

The funds available for the physical/geomorphic monitoring from OWEB were entirely budgeted toward the UAS surveys and supporting field work – laying out geo-referenced targets to support image acquisition as well as establishing and sampling the field validation plots. The larger proportion of the *in-kind* matching funds contributed by the PNW Research Station covered image analyses to be conducted in-house, by PNW personnel.

Changes in staffing after the start of the project severely limited the PNW Research Station's capacity to complete the "*in-house*" image analyses described in the original proposal. Therefore, the PNW Research Station sought external help for several aspects of the project. The PNW used Joint Venture Agreements to contract substantial image analyses to the Oregon State University's Environmental Remote Sensing Applications Laboratory (ERSAL) co-directed by Dr. Michael Wing. Additional support for image analysis was provided via an internal contract from the PNW to the USFS's Geospatial Technology and Applications Center (GTAC). GTAC provided ~200 hours of time from a full-time image analyst who developed and tested protocols to extract inundated area, flow velocity, and sediment size-class distributions from the UAS imagery.

The PNW Research Station's direct cash contributions to this project totaled $71,261 along with at least $22,720 in "*in-kind*" contributions. Additionally, the geospatial analyst support from GTAC was estimated at a value of $20,000. Finally, during the first summer of field work, we had on staff a GeoCorp Intern at a cost of $10,266 to the PNW with an additional $5,764 match from GeoCorp.

Combining all sources of direct monetary costs for the UAS-based remote sensing and supporting image analysis led to a **total direct project cost of $127,291**, of which OWEB contributed $20,000 and the USFS PNW Research Station contributed $107,291, or 84% of the direct costs.

In addition to the direct costs, the PNW made *in-kind* contributions of employees' time and equipment which was originally estimated at $90,500. Additional work undertaken during the project led to further *in-kind* contributions of ~$22,720, resulting in a **total *in-kind* contribution of $113,220**.

DATA STATEMENT:

Stream temperature data have been archived with Oregon Department of Environmental Quality (ODEQ) as required by OWEB and explicitly stated in the contract to the McKenzie Watershed Association. The ODEQ also has the Sample Analysis Plan (SAP) on file; the SAP provides a detailed description of the methods used and other metadata as required by ODEQ.

Currently, all remotely sensed imagery is locally available on the project's work directory and available upon request to collaborating managers working on the project. However, issues of long-term storage remain unresolved. Neither OWEB nor ODEQ have a procedure in place for archiving large files containing remotely sensed imagery. We have approached OWEB with a proposal to complete metadata documentation of these files and store them in a publicly available directory maintained by the US Forest Service. However, doing this will require additional resources because data archival of remotely sensed (UAS) imagery was not planned for in the original project.

ACKNOWLEDGEMENTS:

We thank the Oregon Watershed Enhancement Board for funding and other support for this project, especially Ken Fetcho; we thank the McKenzie Watershed Council for overseeing much of the project organization, especially Jared Weybright; we thank the USFS Region 6 for supporting this project in a myriad of ways, including funding for LiDAR acquisition and other direct funding, especially Brian Staab and Jim Capurso who were instrumental in getting this project started and provided enthusiastic encouragement throughout the monitoring project; we thank the Willamette National Forest and the McKenzie Ranger District for their work on this project, especially Johan Hogervorst, Kate Meyer, Matt Helstab, Mekayla Means-Brous, and Nick Grant; we thank Oregon State University, College of Forestry and its Aerial Information Systems Laboratory where much of the image analysis was conducted; we thank the US Forest Service's Geospatial Technology and Applications Center along with RedCastle Resources, especially Charlie Schrader, and Abigail Schaaf who oversaw the image analysis for inundated area, flow velocity, and streambed sediment. We thank the Geospatial Society of America GeoCorps program that provided significant support for the 2019 field observation campaign. We also thank Lauren Mork and Mathias Perle with the Upper Deschutes Watershed Council for graciously sharing the findings from similar methods implemented at Whychus Creek. Finally, we thank the PNW Research Station who provided funds in direct support of this research as well as substantial *in-kind* support and our PNW Research Station colleagues Becky Flitcroft and Sherri Johnson for having the foresight and vision to advocate having UAS remote sensing monitoring incorporated into the project.